Water-use eciency and transpiration across European forests during the Anthropocene

D.C. Frank[1,2,¶], B. Poulter[3,4,¶], M. Saurer[5], J. Esper[6], C. Huntingford[7], G. Helle[8], K. Treydte[1], N.E. Zimmermann[1], G.H. Schleser[8,9], A. Ahlström[10,11], P. Ciais[4], P. Friedlingstein[12], S. Levis[13], M. Lomas[14], S. Sitch[12], N. Viovy[4], L. Andreu-Hayles[15], Z. Bednarz[16], F. Berninger[17], T. Boettger[18], C.M. D'Alessandro[19], V. Daux[4], M. Filot[20], M. Grabner[21], E. Gutierrez[22], M. Haupt[18], E. Hilasvuori[23], H. Jungner[17], M. Kalela-Brundin[24], M. Krapiec[25], M. Leuenberger[20,2], N.J. Loader[26], H. Marah[27], V. Masson-Delmotte[4], A. Pazdur[28], S. Pawelczyk[28], M. Pierre[4], O. Planells[22], R. Pukiene[29], C.E. Reynolds-Henne[5], K.T. Rinne[5], A. Saracino[30], E. Sonninen[17], M. Stievenard[4], V.R. Switsur[31,†], M. Szczepanek[28], E. Szychowska-Krapiec[25], L. Todaro[19], J.S. Waterhouse[31], M. Weigl[32]

[1] Swiss Federal Research Institute WSL, 8903 Birmensdorf, Switzerland
[2] Oeschger Centre for Climate Change Research, University of Bern, 3012 Bern, Switzerland
[3] Institute on Ecosystems and Department of Ecology, Montana State University, Bozeman, MT, 59717, USA
[4] Laboratoire des Sciences du Climat et de l'Environnement (CEA-CNRS-UVSQ, UMR8212), Institut Pierre Simon Laplace, 91191 Gif-sur-Yvette, France
[5] Paul Scherrer Institute, Villigen, 5232, Switzerland
[6] Department of Geography, Johannes Gutenberg University, 55099 Mainz, Germany
[7] Centre for Ecology and Hydrology, Wallingford, Oxfordshire, OX10 8BB, United Kingdom
[8] Helmholtz-Centre Potsdam. German Centre for Geosciences – GFZ, 14473 Potsdam, Germany
[9] Forschungszentrum Jülich GmbH, 52428 Jülich, Germany
[10] Department of Physical Geography and Ecosystem Science, Lund University, Lund SE-223 62, Sweden
[11] Department of Earth System Science, School of Earth, Energy and Environmental Sciences, Stanford University, Stanford, CA 94305, USA
[12] University of Exeter, Exeter EX4 4QF, United Kingdom
[13] National Center for Atmospheric Research, Boulder, Colorado, 80301, USA
[14] University of Sheffield, Sheffield S10 2TN, United Kingdom
[15] Lamont-Doherty Earth Observatory, Palisades, 10964 USA
[16] Agricultural University, 31-120 Krakow, Poland
[17] University of Helsinki,00014 Helsinki, Finland
[18] Dept. of Catchment Hydrology, UFZ - Helmholtz Centre for Environmental Research, 06120 Halle, Germany
[19] University of Basilicata, 85100 Potenza, Italy
[20] University of Bern, 3012 Bern, Switzerland
[21] University of Natural Resources and Life Science (BOKU),1180 Vienna, Austria
[22] Deptartment of Ecology, Universitat Barcelona, 08028 Barcelona, Spain
[23] Finnish Environment Institute, 00251 Helsinki, Finland
[24] Forestry Museum, 92123 Lycksele, Sweden
[25] AGH - University of Science and Technology, 30-059 Krakow, Poland
[26] Department of Geography, Swansea University, Swansea SA2 8PP, United Kingdom
[27] CNESTEN, 10001 Rabat, Morocco
[28] Silesian University of Technology, 44-100 Gliwice, Poland
[29] Vytautas Magnus University, 44248 Kaunas, Lithuania
[30] University of Naples "Federico II", 80055 Portici, Italy
[31] Anglia Ruskin University, Cambridge CB1 1PT, United Kingdom
[32] Holzforschung Austria, 1030 Vienna, Austria
† Deceased

| Site	Lat.	Lon.	Elev.	Sp.	Type	T(°C)	P(mm)	Tau		Param.	Season	R
COL	32.97	−5.07	2200	CA	C	8.2	467	0.450	[0.380, 0.520]	PET	May	−0.25
CAZ	37.81	−2.96	1820	PN	C	8.2	396	0.595	[0.525, 0.665]	PRECIP	JJ	0.35
SER	39.93	16.20	1900	PL	C	8.5	721	0.760	[0.690, 0.830]	PRECIP	JJA	0.49
PED	42.24	1.70	2120	PU	C	4.8	800	0.620	[0.550, 0.690]	PRECIP	Jul	0.40
LIL	43.07	−5.25	1600	PS	C	5.3	909	0.815	[0.745, 0.885]	TTMAX	JJA	−0.55
CAV	46.35	8.60	900	QP	B	6.4	1868	0.535	[0.465, 0.605]	PRECIP	JJ	0.43
VIG	46.50	8.77	1400	PS	C	4.0	2210	0.445	[0.375, 0.515]	PET	JJ	−0.40
POE	47.95	16.06	500	PS	C	8.0	778	1.470	[1.400, 1.550]	PET	MJJA	−0.31
LAI	48.18	16.20	300	QP	B	9.5	624	1.220	[1.150, 1.300]	PRECIP	JJ	0.45
REN	48.25	−1.70	100	QR	B	11.1	722	0.805	[0.735, 0.875]	RH	Jul	0.47
FON	48.38	2.67	100	QP	B	11.5	591	0.575	[0.505, 0.645]	PET	Jul	−0.60
NIE1	50.12	20.38	190	QR	B	8.4	657	0.470	[0.400, 0.540]	TTMAX	Sep	−0.23
NIE2	50.12	20.38	190	PS	C	8.4	657	0.865	[0.795, 0.935]	PRECIP	Jun	0.32
WIN	51.41	−0.59	10	PS	C	10.0	752	0.615	[0.545, 0.685]	VPD	MJJA	−0.69
DRA	51.50	9.78	320	QP	B	7.5	702	0.925	[0.855, 1.000]	TTMAX	JA	−0.58
WOB	51.98	−0.59	50	QR	B	9.7	698	1.270	[1.195, 1.340]	PRECIP	JJA	0.63
SUW	54.10	22.93	160	PS	C	6.9	599	0.505	[0.435, 0.575]	PET	AMJJAS	−0.55
PAN	54.88	23.97	45	PS	C	6.9	614	0.470	[0.400, 0.540]	TTMAX	JJA	−0.61
LCH	55.27	−3.43	175	QR	B	7.8	1531	1.175	[1.100, 1.245]	PET	JA	−0.46
BRO	60.00	23.08	5	QR	B	5.0	558	0.755	[0.685, 0.825]	RH	JA	0.54
GUT	62.00	12.18	800	PS	C	0.0	643	0.670	[0.600, 0.740]	TTMAX	JA	−0.71
ILO	62.98	30.98	200	PS	C	2.0	569	0.840	[0.770, 0.910]	TTMAX	JA	−0.57
INA	68.93	28.42	150	PS	C	−0.8	422	0.835	[0.765, 0.910]	TTMAX	JA	−0.69

Table S1. *The ISONET dataset spans the European continent and includes a variety of different species from different climatic zones, and with varying sensitivities to climate forcing. Here we provide essential metadata characteristics of all sites ordered by latitude. Columns are: Site abbreviation; Latitude; Longitude; Elevation (m a.s.l.) ; Species (CA = Cedrus Atlantica, PN = Pinus Nigra, PL = Pinus Leucodermis, PS = Pinus sylvestris, QP = Quercus petraea, QR = Quercus robur); Species classification (C = Conifer, B = Broadleaf); Mean annual temperature at site (w.r.t 1901- 2009 baseline); Mean annual precipitation at site (w.r.t 1901- 2009 baseline); Tau ($\delta^{13}C$ / CO_2 ppmv) for best fit with 1st principal component of the 5 instrumental variables for the optimal meteorological season for each site together with lower and upper estimates; Instrumental parameter with highest correlation in inter-annual to decadal domain (RH= relative humidity, PET= potential evapotranspiration, TTMAX = average maximum temperature, VPD= vapor pressure deficit, PRECIP= total precipitation); Meteorological Season with highest correlation in inter-annual to decadal domain (capital letters denote monthly averages over 2 or more months, Single months are indicated by standard three letter abbreviation); correlation with instrumental target after high-pass filtering.*

| Site	TT	TTMAX	PRECIP	RH	VPD	PET
COL	−0.22	−0.24	0.20	0.20	−0.24	−0.25
CAZ	−0.31	−0.29	0.35	0.04	−0.20	−0.24
SER	−0.43	−0.45	0.49	0.39	−0.42	−0.49
PED	−0.31	−0.31	0.40	0.11	−0.22	−0.26
LIL	−0.50	−0.55	0.48	0.31	−0.42	−0.49
CAV	−0.29	−0.28	0.43	0.32	−0.34	−0.29
VIG	−0.39	−0.40	0.35	0.29	−0.32	−0.40
POE	−0.26	−0.30	0.27	0.27	−0.26	−0.31
LAI	−0.39	−0.41	0.45	0.35	−0.39	−0.40
REN	−0.46	−0.46	0.41	0.47	−0.45	−0.43
FON	−0.55	−0.59	0.57	0.56	−0.60	−0.60
NIE1	−0.23	−0.23	0.22	0.17	−0.21	−0.21
NIE2	−0.25	−0.29	0.32	0.17	−0.23	−0.29
WIN	−0.59	−0.67	0.61	0.64	−0.69	−0.68
DRA	−0.52	−0.58	0.45	0.48	−0.56	−0.57
WOB	−0.50	−0.52	0.63	0.37	−0.45	−0.50
SUW	−0.47	−0.53	0.50	0.48	−0.53	−0.55
PAN	−0.54	−0.61	0.38	0.47	−0.56	−0.60
LCH	−0.37	−0.42	0.37	0.38	−0.42	−0.46
BRO	−0.41	−0.46	0.49	0.54	−0.50	−0.53
GUT	−0.65	−0.71	0.43	0.52	−0.64	−0.70
ILO	−0.57	−0.57	0.34	0.38	−0.51	−0.54
INA	−0.67	−0.69	0.30	0.47	−0.63	−0.65

Table S2. *Correlations between high-pass filtered Ci and climate parameters for the optimal seasonal windows. The high pass filtered data were used to assess the primary climatic forcing on isotope discrimination whilst not biasing results based upon long term trends in Ci or climate. Note the correlations are often of similar strength for a variety of instrumental parameters (TT= average monthly temperature, TTMAX= average maximum temperatures, PRECIP = total precipitation, RH = relative humidity, VPD = vapor pressure deficit, PET = potential evapotranspiration).*

| DGVM Model	Photosynthesis Model	Conductance Model	Transpirational Demand	Non-water stressed C_i/C_a	Time Step	Canopy Temperature	Radiation Transfer	Vegetation Dynamic or Static
JULES-TRIFFID	Collatz et al. [1]	Cox et al. [2]	Penman-Monteith [3]	Function of CO_2 compensation point[4]	0.5 hour	Diagnosed from energy balance	Beer's Law	Dynamic
LPJ	Farquhar et al. [5] and Collatz et al. [1]	Haxeltine and Prentice [6]	Monteith [7]	0.8	1 day	Same as air temperature	Beer's Law	Dynamic
LPJ-GUESS	Farquhar et al. [5] and Collatz et al. [1]	Haxeltine and Prentice [6]	Monteith [7]	0.8	1 day	Same as air temperature	Beer's Law	Dynamic
NCAR-CLM4CN	Farquhar et al. [5] and Collatz et al. [1]	Ball et al. [8]	Oleson[9]	0.7	0.5 hour	Diagnosed from energy balance	Two-stream approximation	Fixed
ORCHIDEE	Farquhar et al. [5] and Collatz et al. [1]	Ball et al. [8]	Monteith type [10]	0.667	0.5 hour	Same as air temperature	Beer's Law	Fixed
SDGVM	Farquhar et al. [5] and Collatz et al. [1]	Leuning et al. [11]	Penman-Monteith [3]	0.7	1 day	Same as air temperature	Beer's Law	Fixed

Table S3. *Comparison of DGVM model structures and processes that have direct influence on water-use efficiency as well as model configuration (e.g., static or dynamic vegetation and time step). Additional details on model structure and parameters can be found in Sitch et al.[12], as well as the corresponding publication listed in column 1 (DGVM Model).*
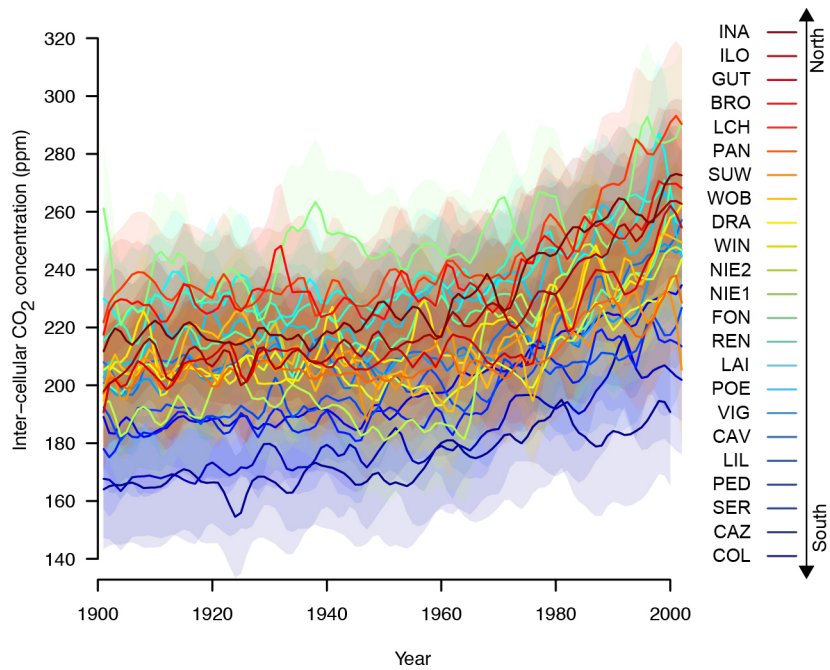
Figure S1. *Site level time series of the inter-cellular CO₂ concentration (C_i) reconstructed from annually-resolved tree ring isotope measurements (see main text and methods for details). Increases throughout the 20th century as well as a latitudinal gradient showing higher C_i moving northwards across the European continent are evident. Time-series were smoothed with a cubic smoothing spline with a 50% frequency cutoff at 5-years to emphasize sub-decadal to centennial variability. Shading shows uncertainty ranges for the individual site level time-series.*
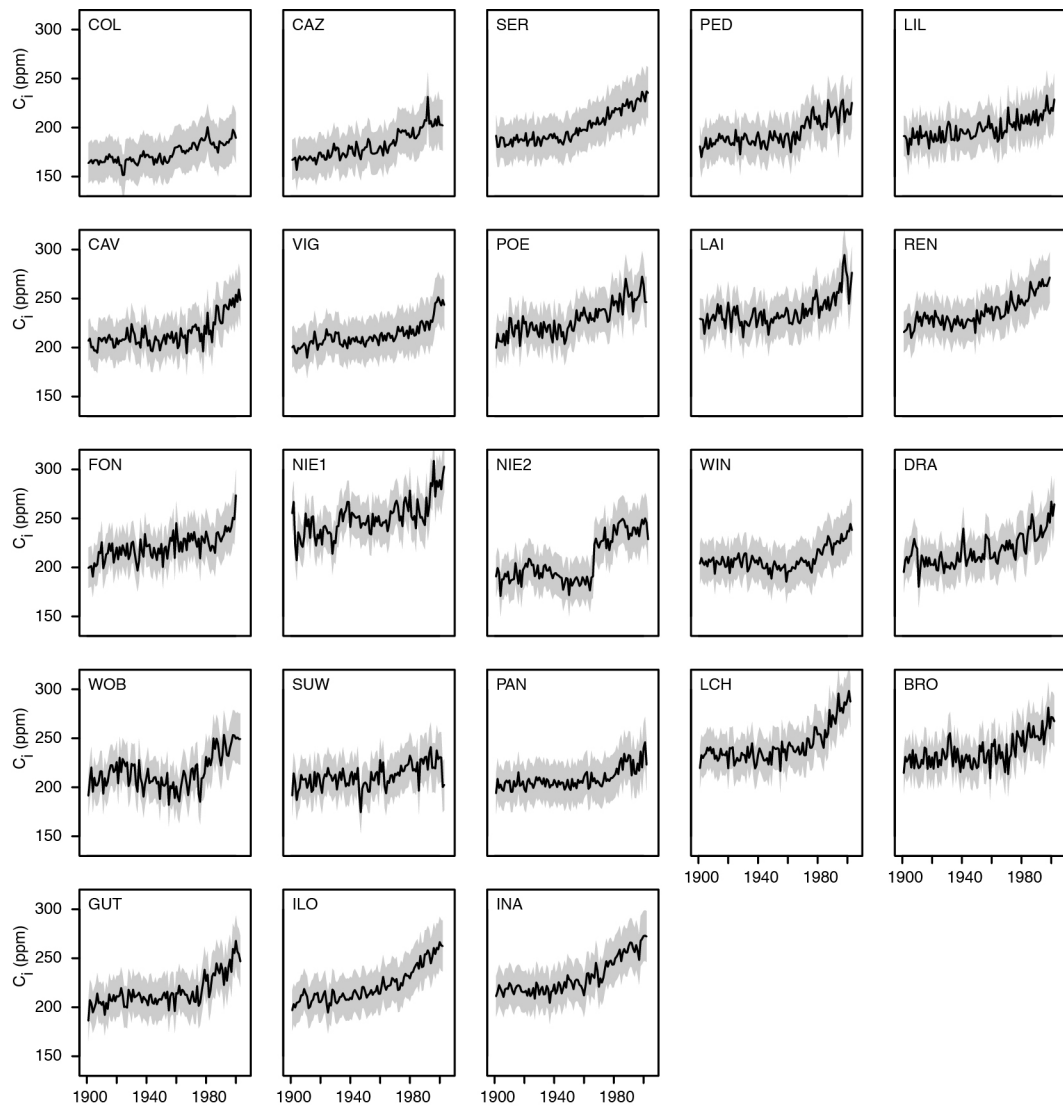
Figure S2. *Site level time series of the intercellular CO_2 concentration (C_i) reconstructed from annually-resolved tree ring isotope measurements (see main text and methods for details). Same as for* **Fig. S1**, *but with annually resolved time-series. Note the overall increasing trend, but also inter-annual to at least multi-decadal variation that is not well explained by the smoother and monotonically increasing concentrations in atmospheric CO_2.*
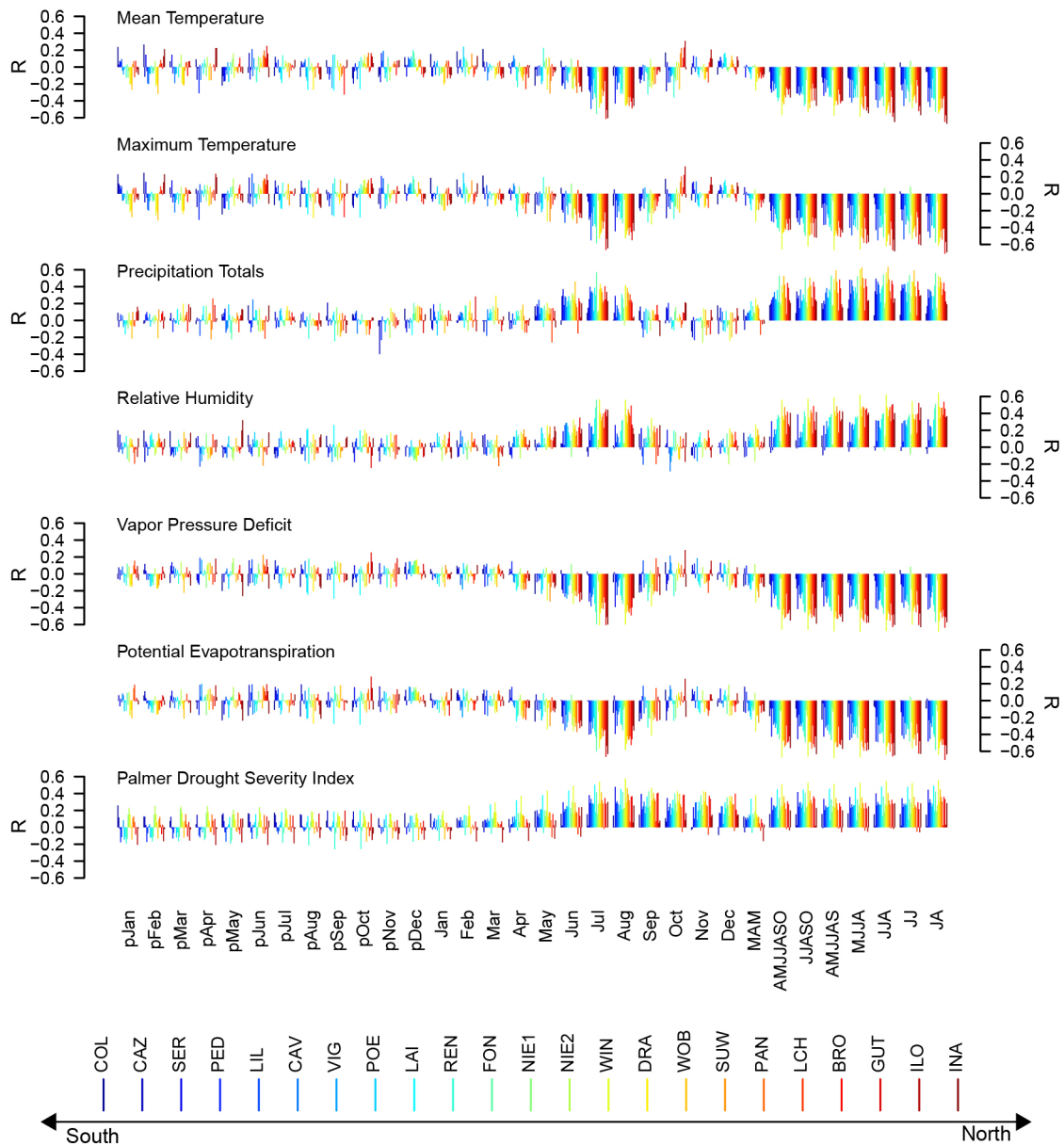
Figure S3. *The annually resolved measurements provide opportunities to quantify the climatic forcing on intercellular CO_2 concentrations (C_i), and thus to differentiate between atmospheric CO_2 and climatic driven effects. Correlations over the 1901-2009 period between the 50-year high-pass filtered C_i and monthly to seasonal climate are provided above primarily using the CRU TS 3.1 dataset and derived parameters. The Palmer Drought Severity Index is from van der Schrier et al. (2006). Correlations are shown for the January prior to ring formation (pJan) to the December after ring formation (Dec), as well as nine seasonal windows (right most columns). Strongest responses are observed during the summer months. Temperature forcing is preferentially enhanced northward (reddish hues), and precipitation towards southern Europe (blue hues).*
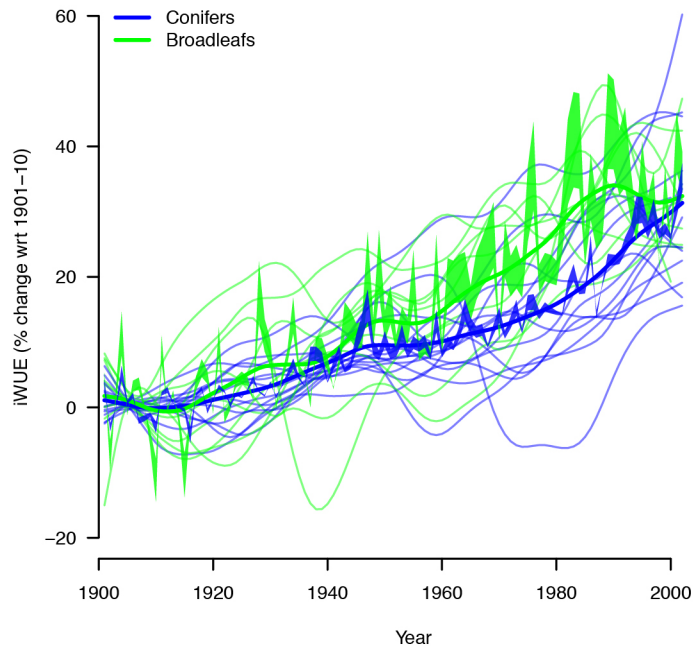
Figure S4. *Changes in intrinsic water use efficiency (iWUE) are commonly derived directly from $\delta^{13}C$ measurements in tree-rings. This approach however assumes that climatic influences on isotopic discrimination are not significant, an assumption directly contradicted by continuing global change and the significant correlations between isotope fractionation and climate (e.g.,* **Figure S3***). Here we show the 20-yr smoothed records to highlight both the increasing iWUE as well as significant (climatically-driven) decadal to multi-decadal fluctuations. Also shown are the means for the conifer and broadleaves (bold) as well as the unsmoothed mean series considering also the uncertainties in isotope discrimination (filled). Assessment of the water use efficiency as percent change minimizes some but not all uncertainties due to factors such as mesophyll conductance and post-photosynthetic isotope fractionation (see supplementary text: uncertainty analysis). To differentiate the climatic versus CO_2 influences on the water use efficiency, we utilized the "tau-approach". See Treydte et al. 2009,* **Figure S5***, and methods.*
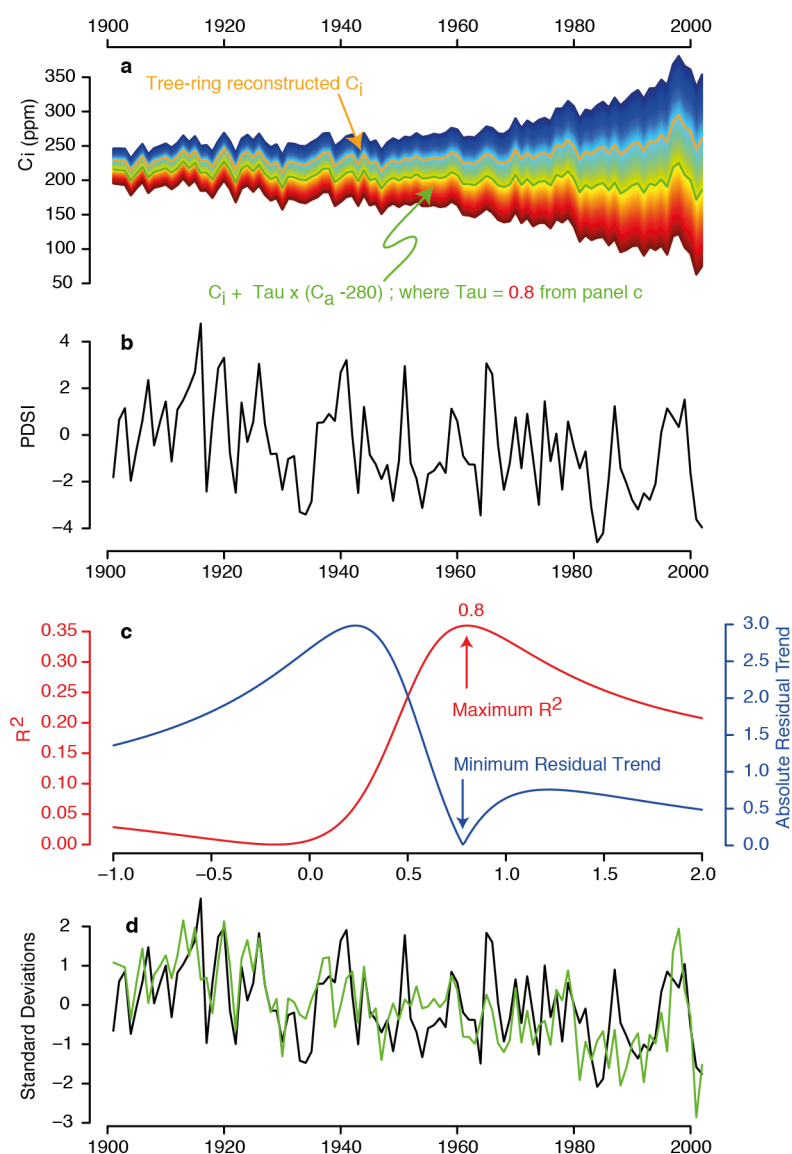
Figure S5. *To isolate the climatic influences on isotope fractionation, a numerical optimization procedure with a control parameter, τ, was performed. This allowed the variance in intercellular CO_2 time-series that were explained by atmospheric CO_2 and climate to be partitioned. Illustration of the "tau approach" for a single site (LAI). a) Reconstructed C_i (yellow+ arrow) together with transforms of the data ((C_i + tau * (C_a-280)) used to identify the τ most consistent with the historical climate (green + arrow). b) Past variations in the Palmer Drought Severity Index showing an increased drying trend. c) Maximization of explained variance and minimization of residual trend were used to determine τ (x-axis); the mean of both τ estimates was considered the best average for the site. d) Fit between the instrumental data (black) and τ adjusted C_i after normalization over the common period. Data for all sites is shown in **figure S7**.*
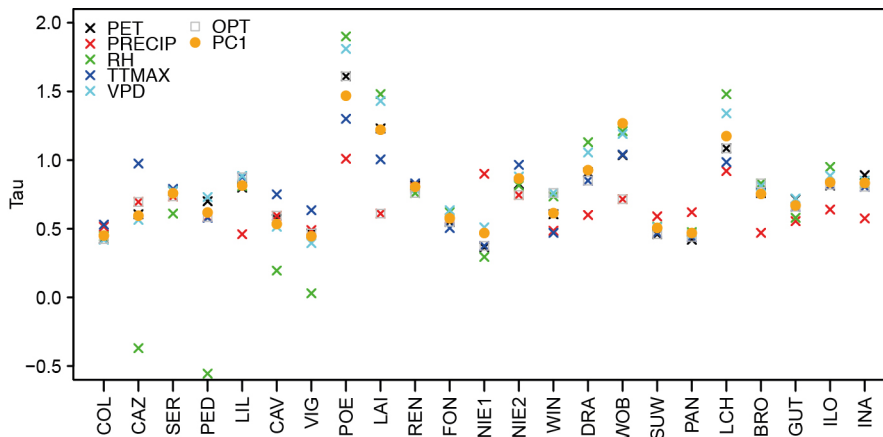
Figure S6. *Tau (τ) estimates for all sites for an array of different instrumental parameters. Shown are the five instrumental parameters from the CRU TS 3.1 dataset from the CRU that correlated highest with isotope discrimination (crosses), as well as their first principal component (circle). The instrumental parameter with the highest correlation after high pass filtering is also highlighted (grey box). This figure highlights variability in site level responses of the physiological response to CO_2 increase, as well as statistical and mechanistic uncertainty associated with estimating τ particularly at higher values, with notable outliers for the relative humidity estimates from southern Europe. Instrumental parameters as in **Table S1**.*
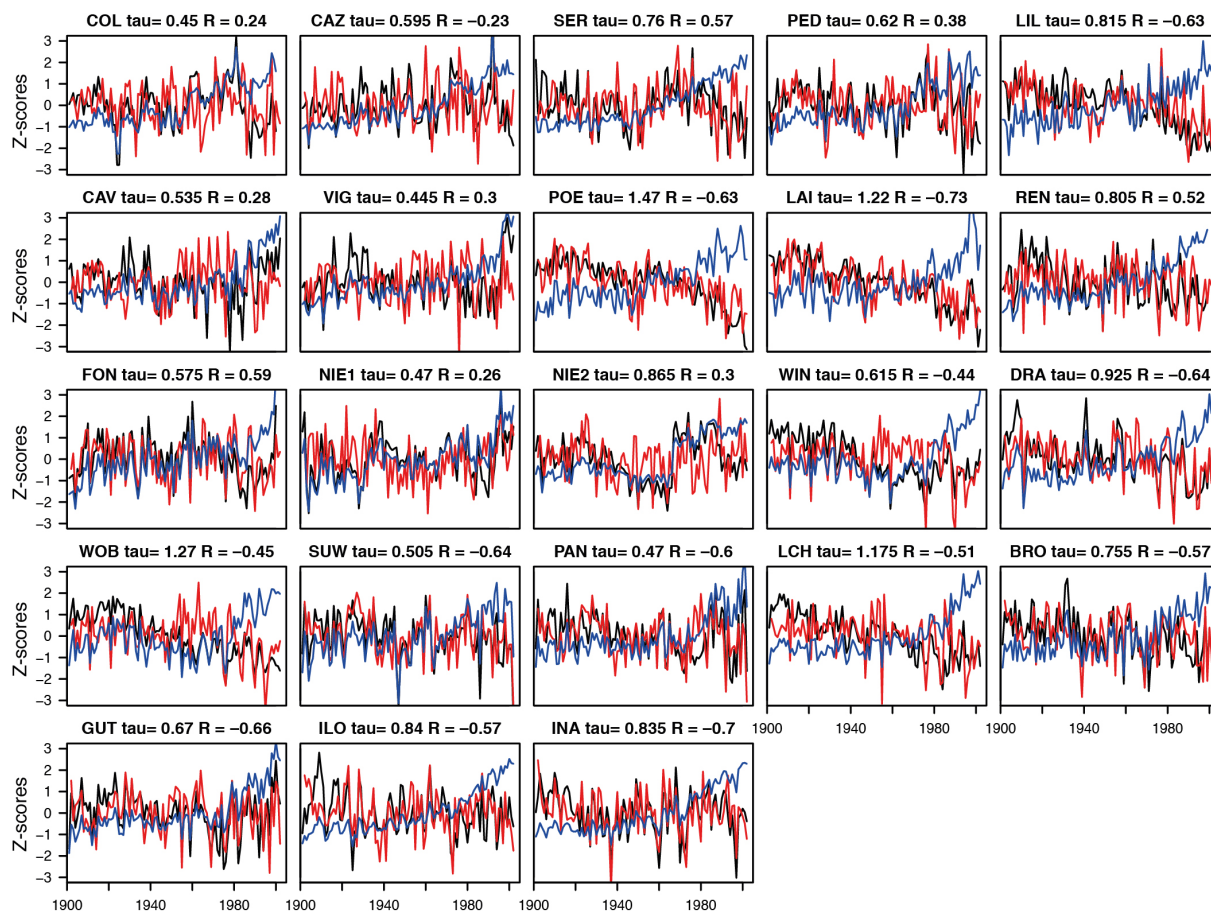
Figure S7. *In this figure we show additional details related to the site-by-site calibration and estimation of τ. Site level changes in C_i (blue) and their corresponding optimizations (black) to the instrumental targets (red). The difference between the blue and black curves represents changes in C_i that are not explained by climate variation and accordingly is used to derive τ (See **Fig. S5** for details). Correlations with the instrumental targets and τ values are shown for each site, with the instrumental data inverted as necessary to enhance visualization.*
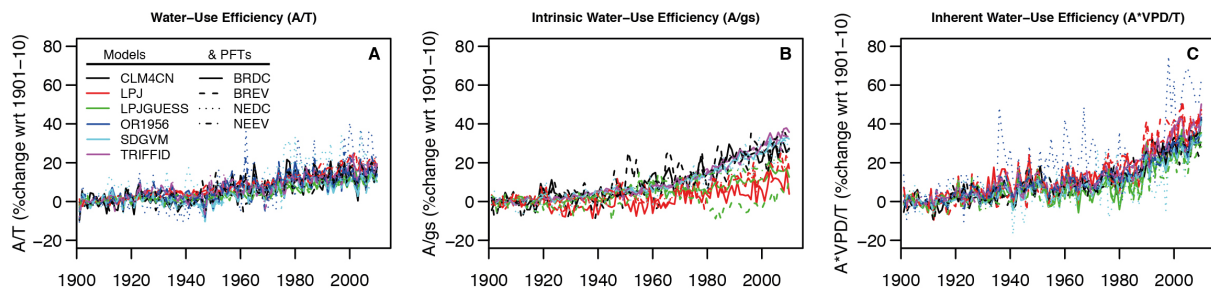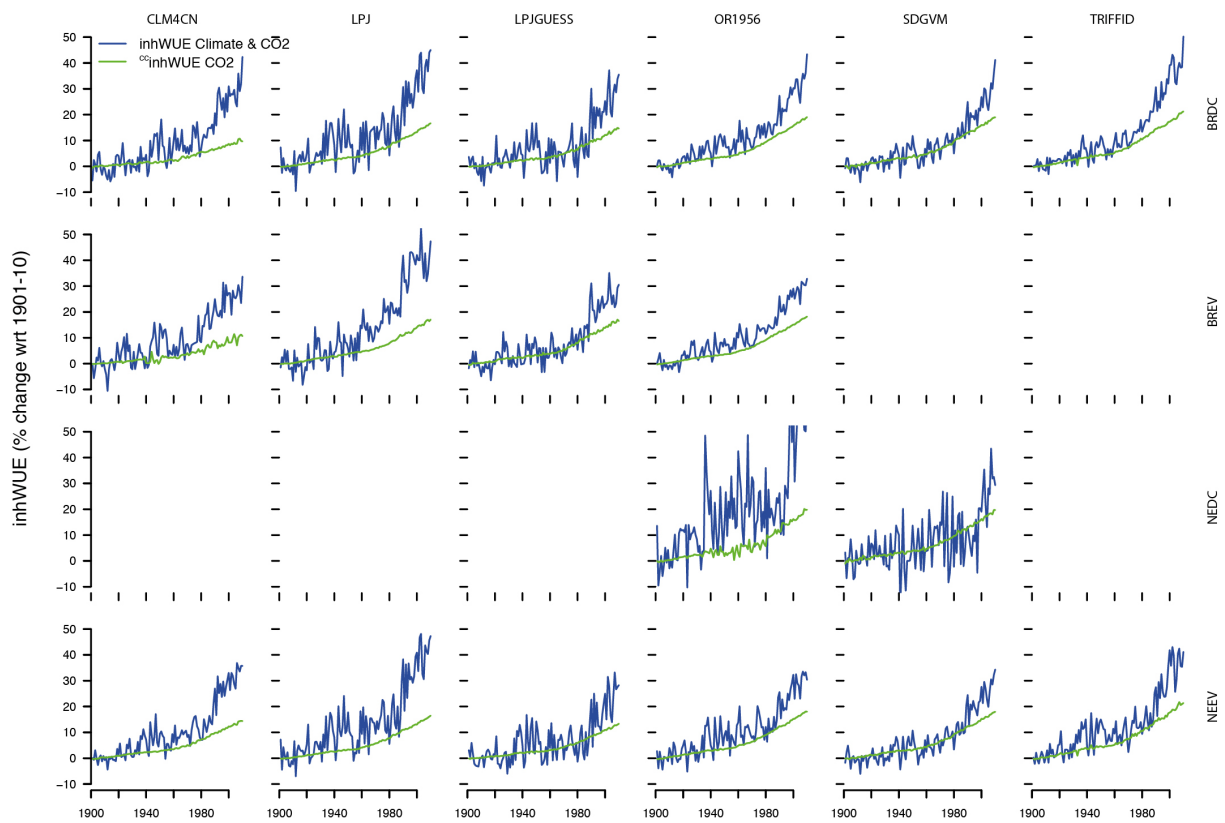
Figure S8. Percent change of WUE metrics for the six DGVM's and four plant functional type categories relative to the first decade of the 20th century (1901-1910). The historical climate and CO$_2$ concentrations (Dyn. Clim. & Dyn. CO$_2$) were used in these model simulations. The plant functional types are: BRDC=Broadleaf deciduous; BREV = Broadleaf evergreen; NEDC = Needleleaf deciduous; NEEV = Needleleaf evergreen. A) WUE defined by assimilation (GPP) divided by transpiration. B) Intrinsic WUE (iWUE) defined by assimilation (GPP) divided by stomatal conductance. C) Inherent WUE (inhWUE) defined by as the WUE multiplied by the vapor pressure deficit. Note greater relative spread in estimates of the iWUE as well as the more rapid late 20th / early 21st century increase of inhWUE driven by rapid warming and increased evaporative demand in Europe during the last decades.
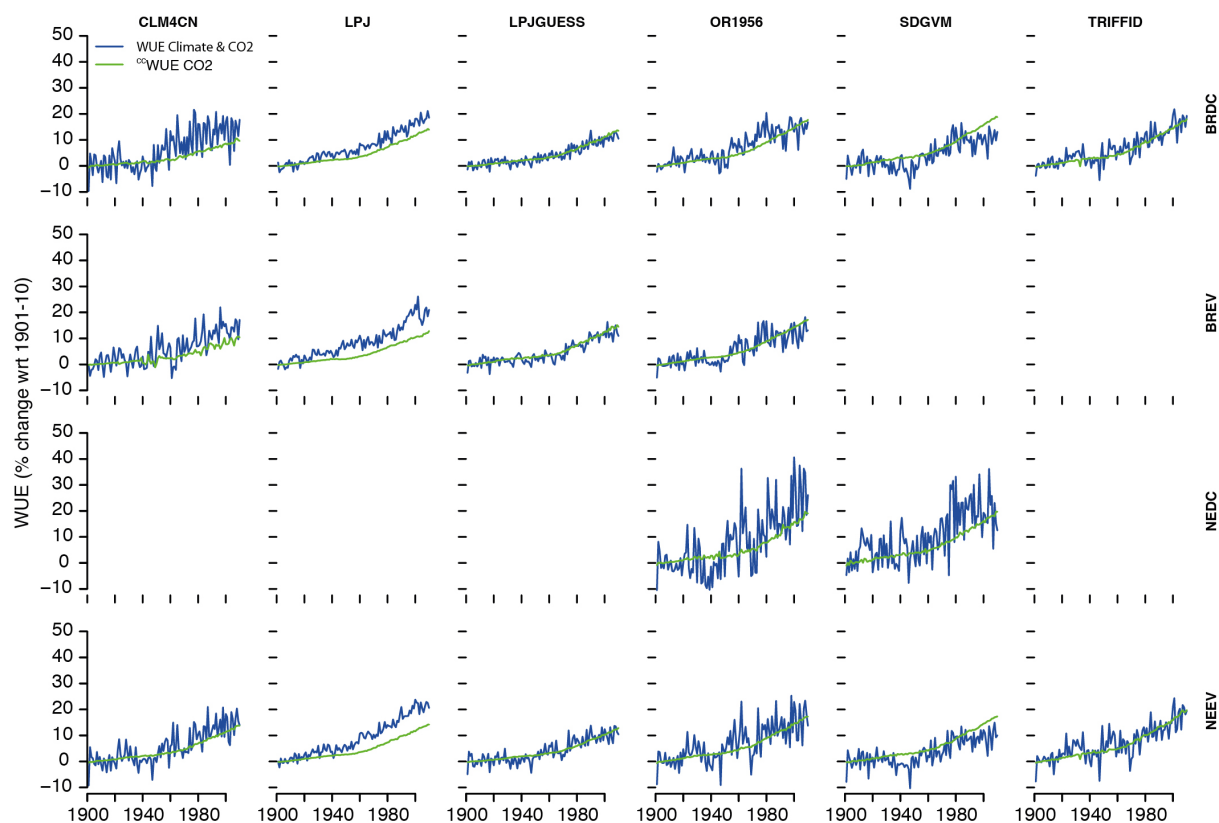
Figure S9. *Comparison of WUE (blue) and "climate corrected" WUE (green) for the six DGVM's and four plant functional type categories relative to the first decade of the 20th century (1901-1910). The plant functional types are: BRDC=Broadleaf deciduous; BREV = Broadleaf evergreen; NEDC = Needleleaf deciduous; NEEV = Needleleaf evergreen. The historical climate and CO_2 concentrations (Dyn. Clim. & Dyn. CO_2) were used to assess the WUE. The standardized difference between the "Dyn. Clim. & Dyn. CO_2" and "Dyn. Clim & "Fix CO_2" after adjusting to the 1901-1910 baseline were used to isolate the effect of CO_2 on modelled WUE.*
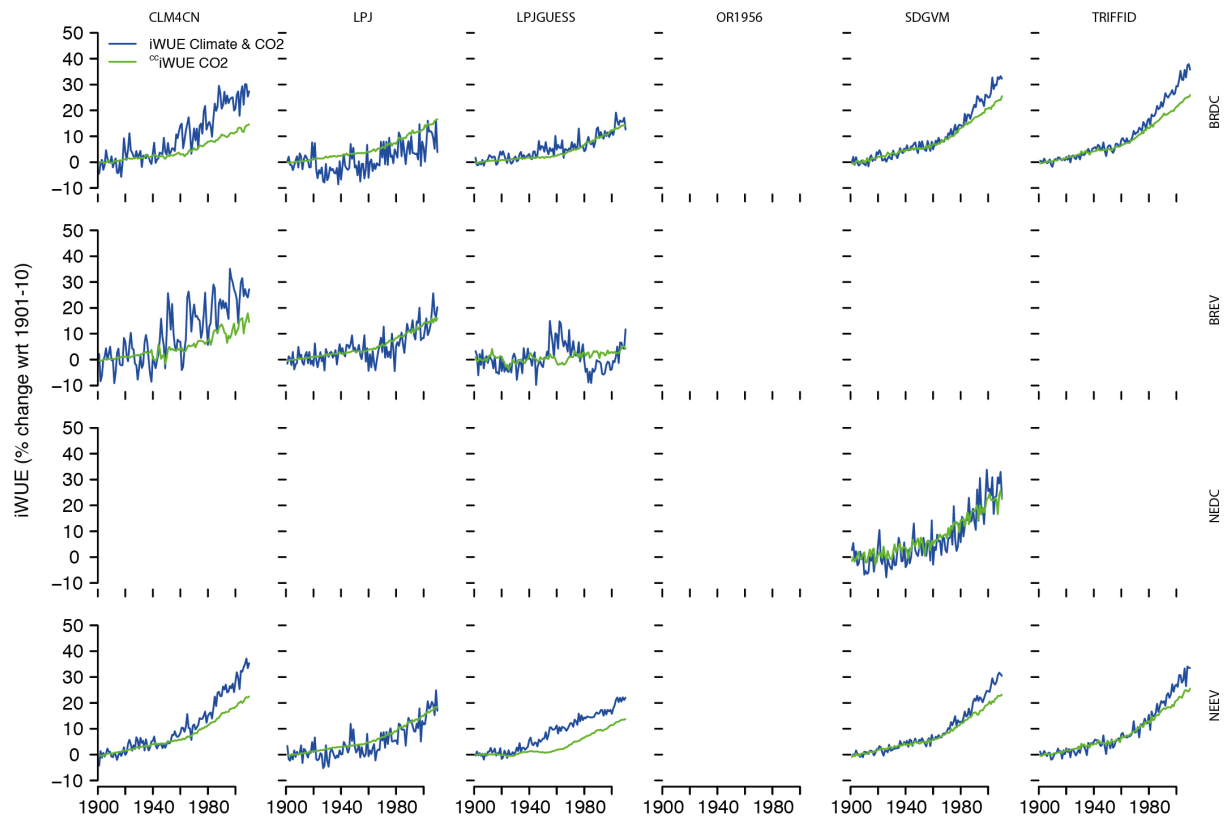
Figure S10. *Comparison of intrinsic WUE (blue) and "climate corrected" WUE (green) for the six DGVM's and four plant functional type categories relative to the first decade of the 20th century (1901-1910). As in Figure S9 but for intrinsic WUE (iWUE).*

Figure S11. *Comparison of intrinsic WUE (blue) and "climate corrected" WUE (green) for the six DGVM's and four plant functional type categories relative to the first decade of the 20th century (1901-1910). As in Figure S9 but for inherent WUE (inhWUE).*
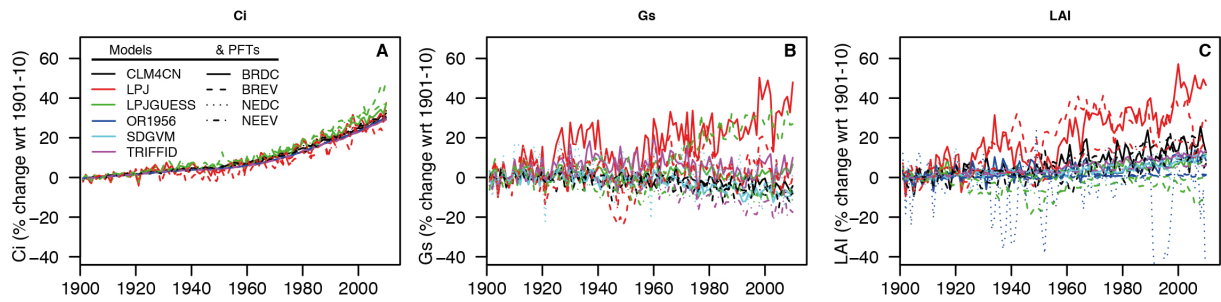
Figure S12. *Percent change of key plant physiological parameters for the six DGVM's and four plant functional type categories. The plant functional types are: BRDC=Broadleaf deciduous; BREV = Broadleaf evergreen; NEDC = Needleleaf deciduous; NEEV = Needleleaf evergreen. The historical climate and CO_2 concentrations (Dyn. Clim. & Dyn. CO_2) were used in these model simulations. A) Intercellular CO_2 concentrations B) Stomatal Conductance and C) Leaf Area Index. The OR1956 simulations provided stomatal resistance and hence values for stomatal conductance are not shown.*
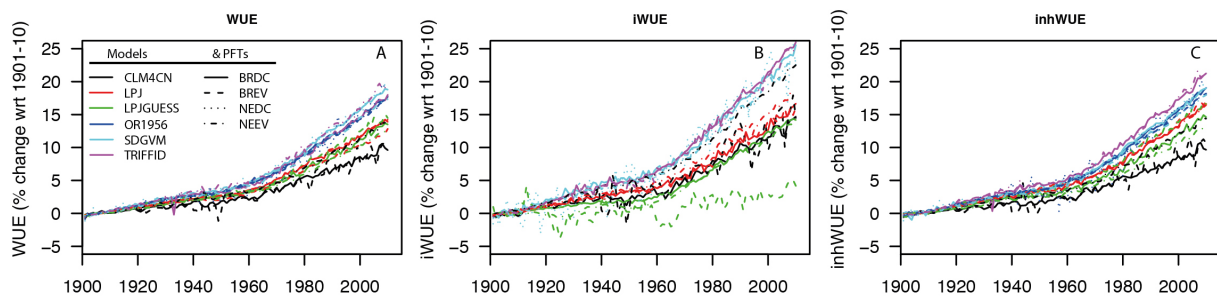
Figure S13. *CO₂-driven increase in various WUE metrics for the six DGVM's and four plant functional type categories. The standardized difference between the "Dyn. Clim. & Dyn. CO₂" and "Dyn. Clim & "Fix CO₂" after adjusting to the 1901-1910 period were used to isolate the effect of CO2 on changes in WUE metrics in these model simulations. A) WUE defined by assimilation (GPP) divided by transpiration. B) Intrinsic WUE (iWUE) defined by assimilation (GPP) divided by stomatal conductance. C) Inherent WUE (inhWUE) defined by as the WUE multiplied by the vapor pressure deficit. The strength of the CO₂ effect is quite similar for all three water use efficiency metrics, although more spread is noted for the intrinsic water use efficiency.*
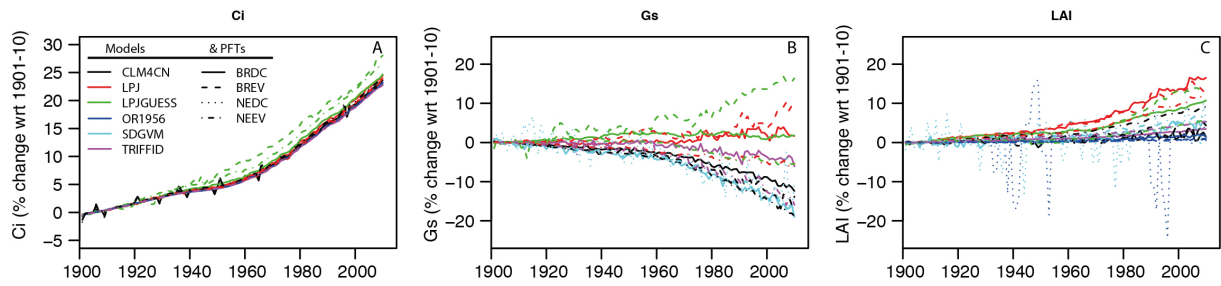
Figure S14. *CO_2-driven increase in plant physiological parameters for the six DGVM's and four plant functional type categories. The standardized difference between the "Dyn. Clim. & Dyn. CO_2" and "Dyn. Clim & "Fix CO_2" after adjusting to the 1901-1910 period were used to isolate the effect of CO_2on changes in plant physiological parameters in these model simulations. A) Inter-cellular CO2 concentrations B) Stomatal Conducance and C) Leaf Area Index. The OR1956 simulations provided stomatal resistance and hence values for stomatal conductance are not shown. Note the different y-axis scale in A).*
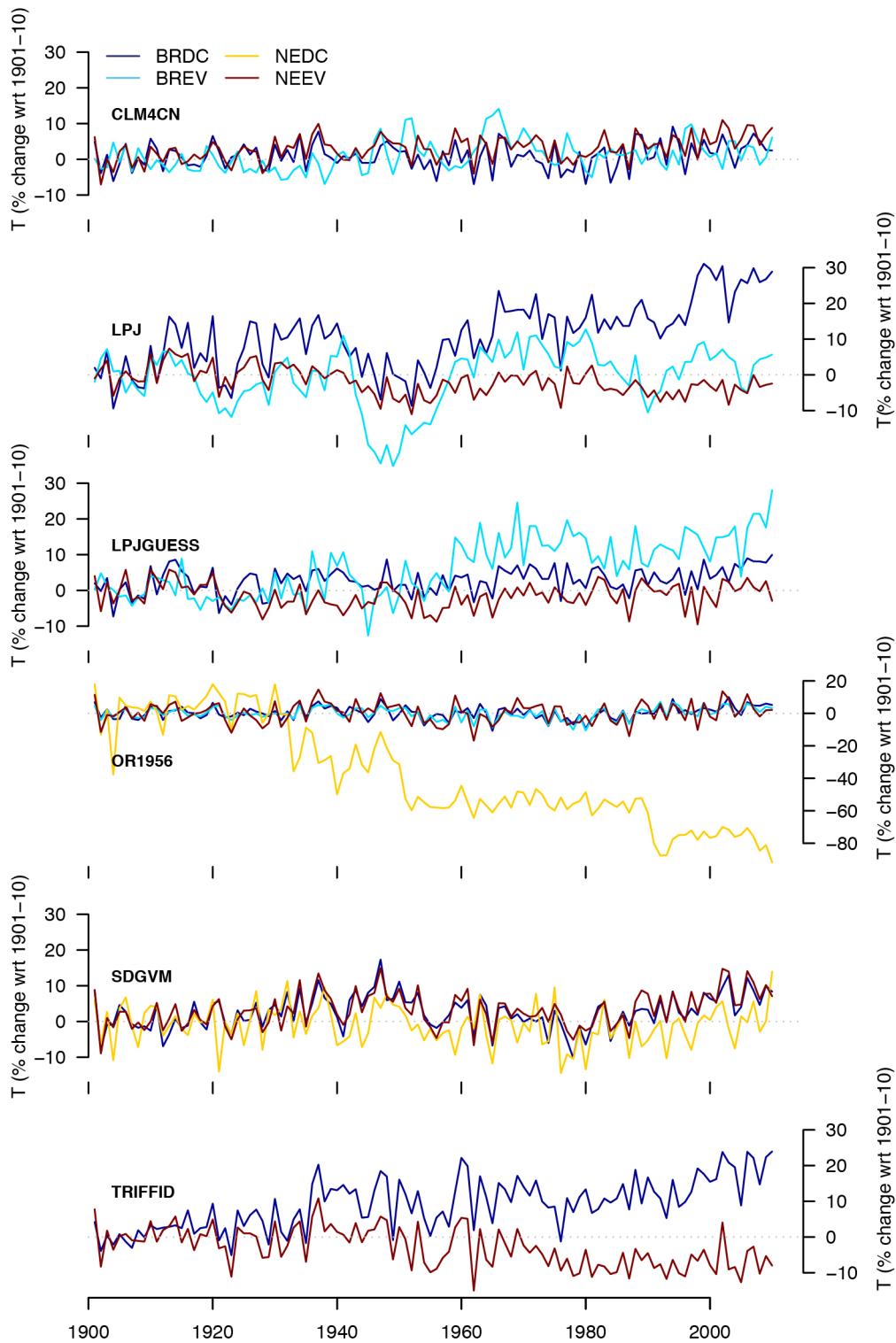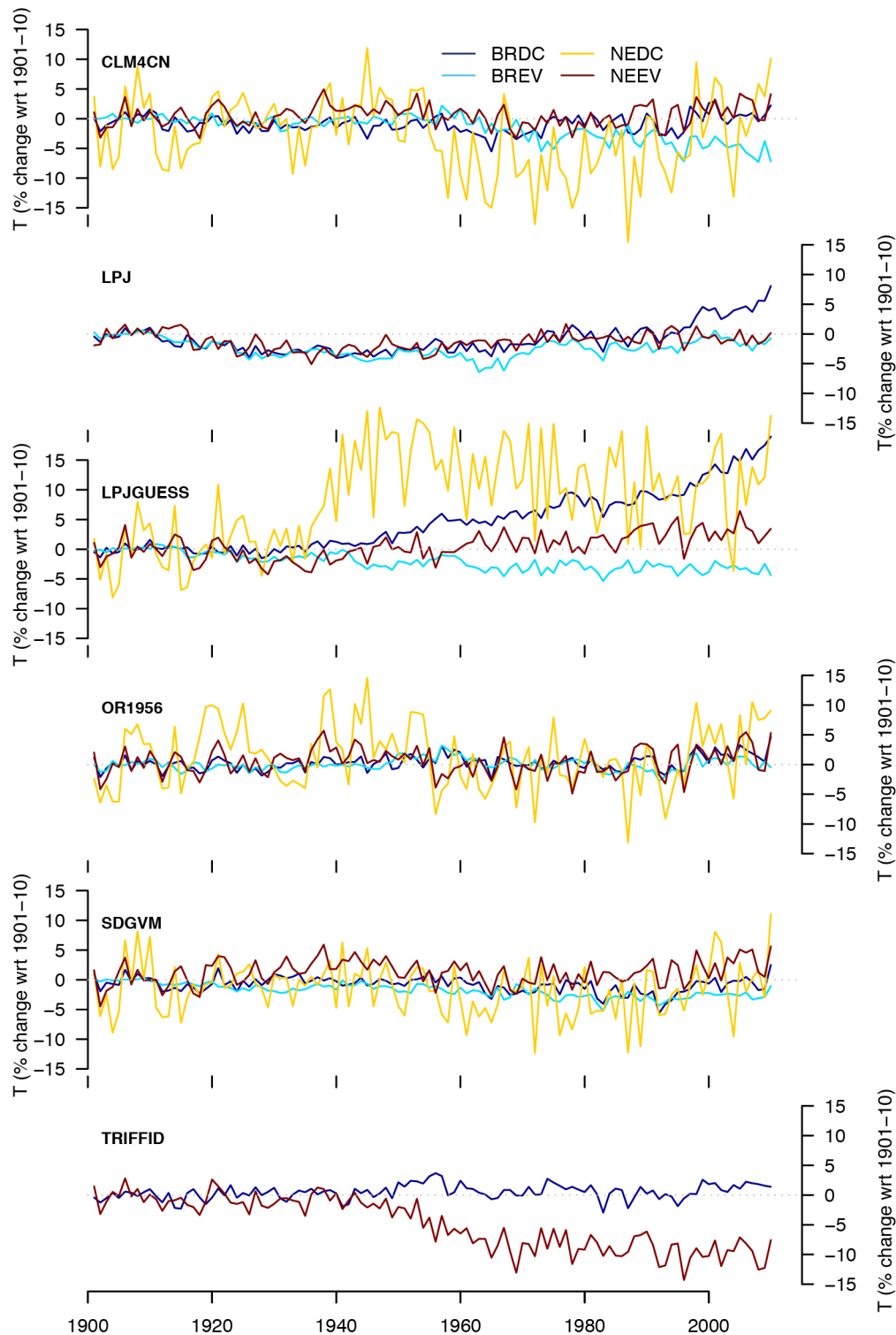
Figure S15. *Percent change of European transpiration for the six DGVM's and four plant functional type categories relative to the first decade of the 20th century (1901-1910). The historical climate and CO_2 concentrations (Dyn. Clim. & Dyn. CO_2) were used in these model simulations. These results suggest that the CO_2 induced reductions in stomatal conductance are generally not strong enough to reduce transpiration. Note the different y-axis scale for the OR1956 results.*

***Figure S16.** Percent change of global transpiration for the six DGVM's and four plant functional type categories relative to the first decade of the 20th century (1901-1910). The historical climate and CO_2 concentrations (Dyn. Clim. & Dyn. CO_2) were used in these model simulations. These results suggest that the CO_2 induced reductions in stomatal conductance are generally not strong enough to reduce transpiration. The modeled evergreen plant functional types tend to show strongest reductions in transpiration, whereas for the deciduous plant functional types both increased leaf area indices and growing season length compensate for decreased stomatal conductance.*
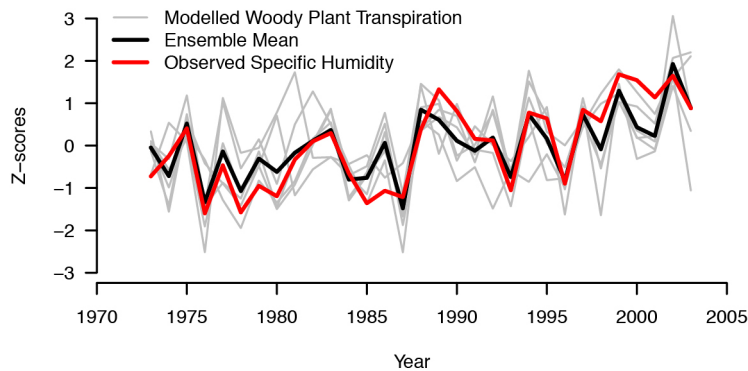
Figure S17. *Changes in transpiration are expected to be coupled with the water vapor content of the air. We test this outcome by comparing the variation in annual woody plant transpiration for Europe (**Figure 3**) with an observational gridded dataset of specific humidity[13]. Although the specific humidity is influenced by numerous processes (snow melt) and regions (lake surfaces) not included in the modeling of woody plants we observe a significant correlation ($R = 0.86$, $p << 0.01$) between the ensemble mean of modeled transpiration and water vapor. This validation lends support to the inferred coupling between the tree-ring empirics, vegetation model results, and land-atmosphere coupling. We note that the forcing data used to run the simulations are independent from the specific humidity observational dataset.*
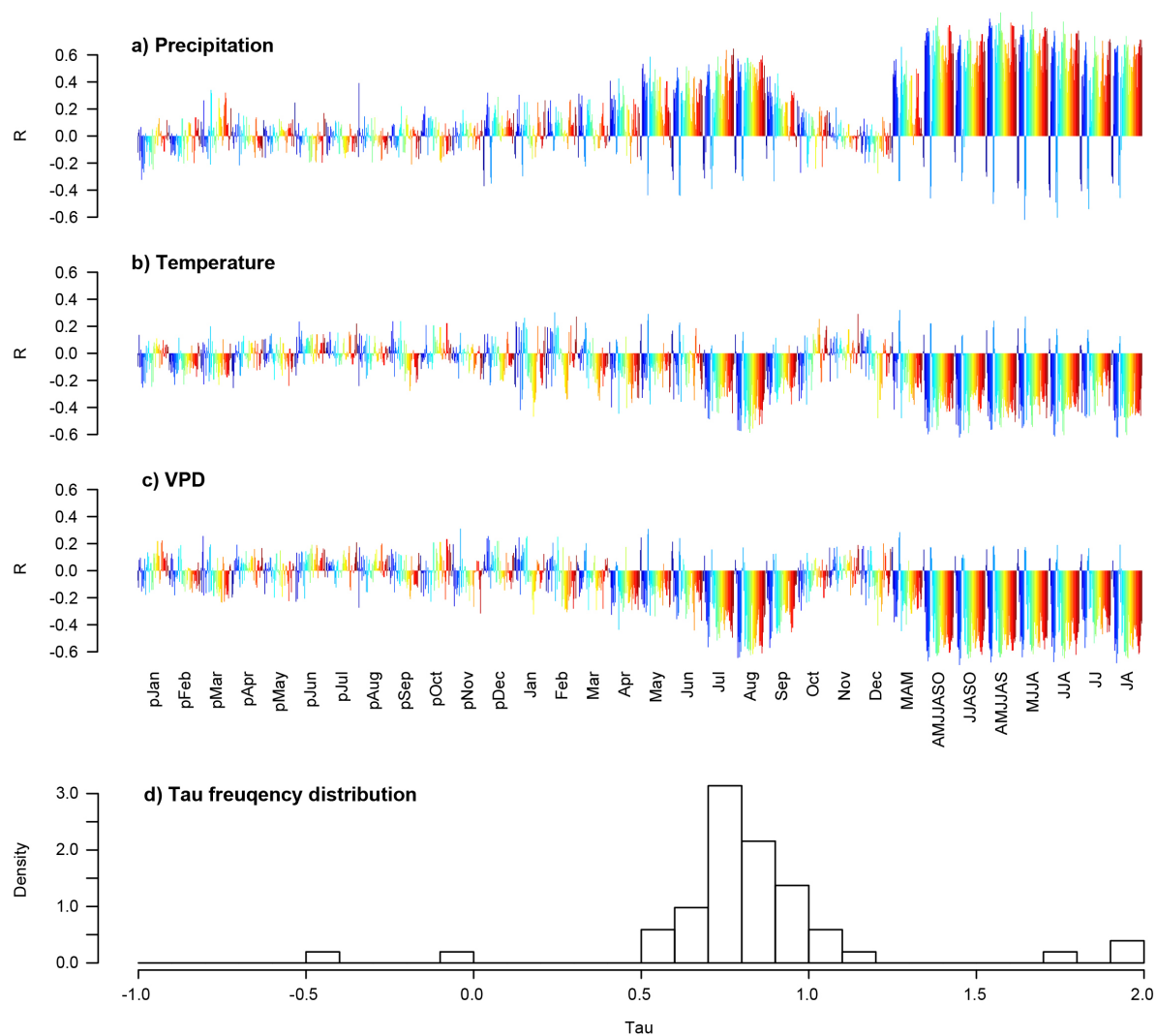
Figure S18. *Derivation of CO_2-only component of Water Use Efficiency using model runs forced by the historical course of climatic and CO_2 variation. Top three panels (a-c) show climatic correlations with a single DGVM run driven by the historical courses of both climate and CO_2 (i.e., "dynamic climate, dynamic CO_2"). Analysis were run at the site level (i.e. at the 23 locations with tree-ring data) using the LPJ DGVM. Different colors (upper 3 panels) represent the combination of different tree PFTs at the individual gridcells. Compare with* **Figure S3** *for empirical-only data. April-September precipitation showed the strongest relationships with the modelled C_i, and was thus used as the climatic benchmark for these validation tests. The lower graph shows the distribution of τ values obtained when removing the climatological influences on C_i (see methods). Compare with* **figure 2**.

FULL METHODS

Tree-ring network and measurements. Data from 23 sites were sampled, measured, and analyzed as part of the European Union funded ISONET project (EVK2-2001-00237). Site selections were based upon criteria including stand age, proximity to measurement locations of the isotopic composition of precipitation, spatial distribution across Europe, and with the exception of the *Cedrus atlantica* site from Morocco are limited to the *Pinus* and *Quercus* genera. These criteria resulted in the preferential selection of sites from non-treeline locations (~75% of the sites), and therefore sites more representative of European forests than typical dendroclimatic datasets. Increment cores were collected from numerous trees at each site, and the annual radial increments were crossdated and measured following standard dendrochronological procedures.

At least two cores from four or more dominant trees per site were selected for subsequent isotope analyses. In detail sample preparation and measurement involved carefully segmenting the cores along annual ring boundaries: for the conifers the full rings were sampled, but for oaks, with the exception of the Swiss site where exceptionally narrow rings prohibited this separation, only the latewood was sampled. For the majority of sites all rings of a given year were pooled together. Subsequent homogenization (milling) and alpha-cellulose preparation followed state-of-the-art and consistent standards[14], with mass spectrometer analysis performed on the CO_2 obtained from combusted alpha-cellulose. $^{13}C/^{12}C$ ratios ($\delta^{13}C$) are expressed as per mille deviations relative to the Vienna Pee Dee Belemnite standard (VPDB). Isotopic discrimination against ^{13}C due to preferential diffusion and carboxylation of ^{12}C, Δ, was expressed as:

$$(1) \qquad \Delta = \frac{\delta^{13}C_{atm} - \delta^{13}C_{tree}}{1 + \delta^{13}C_{tree}/1000}$$

which corrects for the increasingly depleted atmospheric CO_2 composition due to industrial-era fossil fuel emissions[15], where the subscripts *'atm'* and *'tree'* refer to measured isotope ratios in the atmosphere[16] and tree-ring samples. Due to the length of our annually-resolved tree-ring records this correction was performed using smoothed data combining measurements of CO_2 gases trapped in ice-cores with direct atmospheric measurements. While the general trends are expected to be similar, we note that the general geographic position of the sites, the anti-correlated seasonal cycles of both C_a and $\delta^{13}C_{atm}$, and differences in the timing of CO_2 uptake that may additionally relate to the site climatic conditions (**Table**

S1) and deciduous versus evergreen leaf status, may also be expected to have a smaller influence on the C_a and $\delta^{13}C_{atm}$ that the trees experience.

Instrumental data. Maximum and mean monthly temperatures, monthly precipitation, as well as potential evapotranspiration were obtained from the 0.5 x 0.5° resolution CRU TS3.10.01 dataset[17]. For each site the data from the nearest gridpoint were utilized. Relative humidity and vapour pressure deficit were estimated for each gridpoint using the vapour pressure and temperature datasets[18,19]. Corresponding 0.5 x 0.5° gridded Palmer Drought Severity Index (PDSI) data derived from a prior versions of the CRU dataset were utilized[20] for additional comparisons but were found to generally explain less variance in the isotope data than the other instrumental parameters. Correlations with tree-ring data were computed over the maximum possible period of overlap between 1901-2010 with all tree-ring sites having data at least until 1999 (N=99).

Calculation of intercellular CO$_2$ concentration. Following ref. [21], the isotopic discrimination in C3 plants is proportional to the intercellular to atmospheric concentrations of CO_2 (C_i and C_a, respectively):

$$(2) \qquad \Delta \cong a + (b - a)\frac{c_i}{c_a}$$

where 'a' and 'b' are determined constants associated with fractionation due to diffusion and carboxylation, with values of 4.4‰ and 27‰, respectively. See text for details. Equation (2) then shows how the isotopic discrimination can be used to estimate the ratio of the intracellular to atmospheric CO_2 concentrations (C_i/C_a), which may be regarded as an important homeostatic set point for plants. Equation (2) may alternatively be solved for C_i when considering longer term atmospheric and ice core measurements of C_a, as done in this study. These gas exchange and discrimination processes also are fundamentally linked with the iWUE of plants[22].

The above (eq. 2) formulation of the Farquhar isotope discrimination model is applicable for the primary photosynthetic assimilates in the leaf and does not consider downstream post-photosynthetic fractionation due to processes including synthesis of secondary sugars, respiration, compound exchange within the phloem, starch storage and subsequent remobilization and incorporation in the wood structure ([23-25]). These post-photosynthetic processes are to some extent reflected in the compound and organ specific fractionation,

measurements of which can be used to both improve estimation of iWUE from tree-ring material and quantify associated uncertainties. We accordingly consider a modified version of the above discrimination model (e.g., [24,26]).

$$(3) \qquad \Delta \cong a - d + (b - a)\frac{c_i}{c_a} + \varepsilon$$

The term d is employed to sum discrimination (d_1, d_2,…,d_n) beyond those associated with the direct photosynthetic production of triose phosphates and ε represents variability among trees within a site. Considering current knowledge and available data, we characterize the post-photosynthetic fractionation based upon measurements of the isotope composition available for the leaves (d_1), in the bulk wood material (d_2), and in the alpha-cellulose (d_3) with values of d = 2.1 ± 1.2‰ and ε = 0 ± 0.8‰. The individual d terms as well as ε are estimated from a survey of literature and meta-data reviews (see supplementary material). The errors are assumed to be normally distributed, independent and propagated in quadrature and rounded up with the sum of the d and ε terms to be -2.1±1.5 ‰. We use Δ' to refer to isotope discrimination values after correction of the tree-ring alpha-cellulose data for post-photosynthetic discrimination. Δ' should provide improved estimates (and associated uncertainties) for the leaf level processes in comparison to the uncorrected whole wood or cellulose measurements.

Despite these improvements, note the approximate equality symbol in equations 2 and 3. It has been pointed out[22,27], that other factors such as changes in mesophyll conductance or the temperature sensitivity of enzymatic discrimination may modify these basic relationships. For example, a review by ref. [28] showed that a component of diffusion, mesophyll conductance, itself can be understood as a function of diffusion through liquid phases, cell walls, and the intra-cellular spaces. These factors appear to change as a function of tree/leaf age, environmental conditions, and among species. Evidence suggests that these multiple processes vary in response to environmental variation similar to responses of the stomatal conductance[28], but more work is needed to test this especially over inter-annual time-scales. Even though the individual physiological processes that drive isotope discrimination may not be easily differentiated, the climatic dependence of these processes will be considered in the "tau-approach" implemented in this study (see "Removal of climatic effects on water use efficiency" section) thereby improving understanding for the CO_2 influences on isotope discrimination and tree physiological processes. Furthermore, as the discrimination constants used above implicitly include such factors, and neither the knowledge how to specifically

correct for intertwined climate, physiological, and ontogenetic effects, nor the necessary physiological time series are available for the different species/sites within the network, we utilize the first order approximation. We note that the Dynamic Global Vegetation Models utilized in this study (see below) incorporate a similar level of aggregation of physiological processes. Detailed physiological measurements and attribution of changes over time to aging and/or climatic and/or environmental effects for a variety of species will allow improved simulations and empirical studies. Such efforts in the coming decade may yield possible refinements on the magnitudes, but unlikely the directions, of plant responses to both climate and CO_2 variation in the atmosphere.

Calculation of water use efficiency. The plant stomata, which regulate the exchange and diffusion of CO_2 and are responsible for initial isotope discrimination, simultaneously regulate the transpiration and plant water loss. Thus the isotopic measurements can be used to study the water use efficiency – the amount of carbon fixed per unit of water lost. The so-called intrinsic water use efficiency (iWUE) is the ratio of the assimilation rate (A) and stomatal conductance of water vapor (g).

$$(3) \qquad iWUE = \frac{A}{g} \cong \frac{C_a(b-\Delta')}{1.6(b-a)} \cong \frac{1}{1.6}(C_a - C_i)$$

This ratio is driven by the difference in partial pressures between the atmospheric and intracellular CO_2 concentrations (C_a and C_i, respectively), and can in turn be related to the measured values of isotopic discrimination (Δ or Δ').

The iWUE is regarded as a potential water use efficiency estimate at the leaf level rather than a whole plant or ecosystem assessment because i) iWUE does not account for losses of assimilates due to respiration and ii) environmental changes, that for example, increase or decrease the vapour pressure deficit, will also influence the actual plant water loss. In our investigation we assess climatic influences on isotopic discrimination including changes in leaf conductance to CO_2 via the "τ approach" (see below) as well as climatic influences on transpiration via a modelling approach (see main text for details). We do not address possible changes in plant respiration. Estimates of iWUE based upon the GPP/Gc, estimates of WUE based upon GPP/transpiration, and estimates of the inherent WUE (ref. [29]) based upon (GPP*VPD)/Gc were derived from the Dynamic Global Vegetation Model (DGVM)

simulations (see below). GPP refers to the gross primary production. A comparison of these three WUE metrics showed subtle differences in the magnitude of trends related to how stomatal conductance relates to transpiration and the influence of VPD increases throughout the 20th century on WUE (**Figures S8 & S13**).

Removal of climatic effects on water use efficiency. As we are primarily interested in isolating the how increased atmospheric CO_2 concentrations (C_a) affects tree physiology and the leaf to atmosphere CO_2 gradient, quantification of how intercellular CO_2 concentrations (C_i) of trees has changed since industrialization is of particular relevance. However to isolate the C_a impacts on C_i, it is first necessary to remove the influences of climate variation from the isotope records. This point is evident when considering the i) significant short to long-term changes in climate over the past century and ii) the utilization of carbon isotopes to reconstruct these climatic variation[30-32]. Accordingly, and following the general procedures outlined by ref. [30], we screened the 50-year high passed filtered (i.e., removed long-term trends and retained primarily inter-annual to multi-decadal variability by computing residuals from a smoothing spline) C_i time-series against a variety of climate parameters and monthly and seasonal windows. The high-pass filtering was performed as to avoid influence of trends on inferred relationships, which would later complicate the attribution of possible long-term responses to C_a. The optimal seasonal window for five parameters (mean monthly temperatures, maximum monthly temperature, potential evapotranspiration, and vapour pressure deficit) were estimated for each site from the correlations coefficients and considered for further analysis both individually as well as the first principal component of the meteorological parameters for each site. C_i time-series were then adjusted by adding a time varying CO_2 component that is a linear function of atmospheric CO_2 concentration above a pre-industrial baseline ($C_i + \tau * (C_a-280)$). See **figure S5** for an example of these calculations. The use of the control parameter, τ, allowed us determine to what extent the trends in C_i were explained by the unfiltered climatic data, and hence determination of the residual long-term component indicative of a physiological response. Specifically τ was varied within the range from [-1,2]. The full τ-dependent suite of time-series for each site was then regressed upon the optimal climatic target to determine which value of τ yielded i) the highest explained variance and ii) a model residual time series with the smallest trend – these two estimates were averaged. Only the explained variance estimates were used in the 9 out of 151 cases where a local minimum slope could not be determined for the linear estimation. The primary advantage of this method in comparison to, for example, direct removal of the temperature

effects via linear regression, is that we explicitly account for low frequency changes in estimating plant response, but not in the climatic screening. In addition to **Figure S5**, examples of the τ calculations are provided in ref. [30]. In some cases the "optimal" instrumental parameter for analysis yielded only slightly higher correlations than other instrumental parameters (**Table S2**). We accordingly show results separately for all individual parameters and their first principal component as the best estimate. We find the overall distribution τ estimates (**Fig. 2c**) is not sensitive to these choices. However, outlier estimates for certain sites and parameters exist (**Fig. 2c** and **Fig. S5**), so we thus consider the mean/median τ values for the broadleaf and coniferous to be the most robust estimate for changes in iWUE in European forests (**Fig 3a**).

As this "τ approach" can be used to estimate long-term changes in C_i or iWUE where effects of climatic are corrected for, we use the superscript prefix notation $^{cc}C_i$ and ^{cc}iWUE to refer to C_i and iWUE values where climatic influences on empirical quantification have been considered. A τ value of minus unity means that for every ppmv increase in C_a, the $^{cc}C_i$ would actually decrease by the same amount. A τ value of zero means that the plants have maintained a constant $^{cc}C_i$, and a τ value of unity means that for every ppmv increase in C_a, the $^{cc}C_i$ increases by the same amount. The τ values, which quantify the relationships between $^{cc}C_i$ and C_a were then converted into ^{cc}iWUE estimates using the relationships shown in equation (3). A τ value less than unity is indicative of an increase in ^{cc}iWUE.

A test of these empirical methods using the "dynamic climate, dynamic CO_2" model simulations showed that we were able to recover the magnitude for the increase in CO_2-only driven variation in C_i, albeit with uncertainty related to statistically estimating and eliminating the climatic controls on C_i (**Figure S18**). Our tests are consistent with the empirical findings shown in **Figure 2** and support conclusions that also the physiological response of trees also to a long-term increase in CO_2 concentrations is most consistent with maintenance of a constant C_i /C_a. We observed that correlations between climate and the tree-ring data were generally comparable to the climatic correlations with modelled iWUE or C_i, yet tended to be more consistent across Europe even though the models were driven by these same climatic data. The "tau" approach performs particularly well where a high correlation exists between the C_i and climate (see **figures S3** and **S7**).

Even though the consideration of climatic effects on C_i and iWUE should yield notable improvements in quantifying CO_2-driven changes in plant physiological processes, this

approach is not without possible limitations. Uncertainty in the τ estimates derives from identifying the climatic drivers responsible for inter-annual to long-term changes in isotope discrimination (**Fig. S3**), statistical uncertainty in the estimation procedure (**Fig. S4 – S5, S18**), the absolute values of C_i (**Figs. S1-S2**), as well as those variations in the C_i driven neither by climate nor atmospheric CO_2 (ref. [33]), and inhomogeneities in the instrumental data themselves[34]. Climate effects on isotope discrimination are limited to evaluation of climate parameters whose effects are assumed to be linear and stable over time. The same is assumed for relationships with CO_2, which based upon experimental data is reasonable for the concentrations experienced in the past[35], however not well tested in natural environments. Furthermore the low frequency variation in the tree-rings is assumed to reflect a linear combination of the climatic response and physiological response to CO_2 variation. Possible pollution effects in the tree-rings[33,36] or inhomogeneities in the instrumental data[37] are regarded to be secondary to the CO_2 and climatically driven effects on isotope discrimination. Suggestions that pollution effects are of a highly local nature[33] will need further testing and require the development of more spatially dense networks within Europe[38]. Similarly, further investigations from other regions across the globe including minimally polluted (e.g., sulfur, nitrogen) areas and those with variable pollution histories, different long-term changes in climate, and ideally long and robust climate and pollution records will be helpful to confirm and refine the physiological effects to increased CO_2 we observe across Europe.

Dynamic Global Vegetation Model (DGVM) Simulations. Vegetation model simulations were performed to i) quantify the degree to which the different models meet empirical iWUE estimates and uncertainties therein and ii) provide insights on transpiration due to climate varability and the plant response to CO_2. An ensemble of six state-of-the-art DGVMs (**Table S3**) were included in our study: LPJ (ref. [39]), LPJ-GUESS (ref. [40]), JULES-TRIFFID (ref. [4]), SDGVM (ref. [41]), ORCHIDEE (ref. [42]), NCAR-CLM4CN (ref. [43]). Model analysis is an offshoot of the TRENDY Intermodel Comparison ("Trends in net land-atmosphere carbon exchange over the period 1990-2009") that was launched to provide bottom up estimates of carbon cycle processes for the regional synthesis of the REgional Carbon Cycle Assessment and Processes (RECCAP). Accordingly, quantification of regional trends and variability in the carbon cycle from the TRENDY initiative can be found elsewhere[12,44]. For our study on water-use efficiency, six modelling teams (out of 9 in the overall TRENDY project) participated (**Table S3**) by following a strict modelling protocol that outlined simulations for three factorial experiments (denoted S1, S2, S3) using observed climate, CO_2, and land use and land cover change over the period 1901-2009 to drive the DGVMs. Our analysis uses

model data from the "S2" storyline that includes time varying atmospheric CO_2 concentrations and climate and time invariant land use for 2005. We refer to this set of simulations as the "dynamic climate, dynamic CO_2" as both factors followed their historical courses. A fourth experiment (S4) designed especially to evaluate trends in water-use efficiency for this work was performed to isolate the effects of CO_2 on plant physiology, control simulations using historical climate but time invariant CO_2 concentrations fixed at pre-industrial levels (287.14 ppm; "dynamic climate, fixed CO_2"). The standardized difference between the "dynamic climate, dynamic CO_2" and "dynamic climate, fixed CO_2" simulations (as anomalies relative to the 1901-1910 period) were used to isolate the effect of CO_2 on changes in WUE metrics in the model simulations (e.g., as plotted in Figure 3a). Model differences are assumed to provide an estimate for the CO_2-only effect.

DGVM forcing datasets, configuration and analysis. The CRU-NCEPv4 climate dataset was used to provide DGVM models with climate forcing variables at 6-hourly resolution for the years 1901-2010, including precipitation, snowfall, temperature, shortwave and longwave radiation, specific humidity, air pressure and wind speed. Global atmospheric CO_2 was provided as an annual time series reconstructed from ice-core measurements that are then merged with direct observations starting in 1956 from the Mauna Loa record. Land use distinguished between managed crops and natural vegetation using a common database[45] with land use fixed for the year 2005 for all simulations is used in our study. Modelling groups used their own soil database to specify soil texture, water holding capacity, and thermal diffusivity properties (typically as specified by the Food and Agriculture Organization[46]). Modelling groups also individually determined the treatment of vegetation dynamics and natural disturbances, using either static or dynamic plant functional types and including or excluding disturbance (mainly fire). Models were spun-up to equilibrate soil and vegetation carbon pools for pre-industrial conditions (typically 1000-3000 years) by recycling climate mean and variability for years 1901-1920. The simulations were then initialized[47] with the final spin up configuration. European and Global land areas were defined according to the Transcom III delineations.

Model structure and response. The ensemble of DGVM models provides an opportunity to evaluate the role of structural uncertainties on trends in water-use efficiency. Differences in model structure arise when there is uncertainty in the physical basis of ecophysiological processes and vegetation dynamics. **Table S3** presents the main processes related to determining water-use efficiency, A/Gc, where A is carbon uptake and Gc is stomatal

conductance. In most cases, the models all base photosynthesis on a well-established biochemical model[48]. The Farquhar model estimates the enzyme kinetics of Rubisco, the main enzyme limiting photosynthesis, based on available light, temperature, and leaf internal CO_2 concentrations. The type of stomatal conductance model varies between the models because there are various perspectives on the main environmental drivers that determine stomatal aperture. For example, some models emphasize the coupling of soil moisture with stomatal conductance (e.g., ref. [6]) where as other models favor a more direct influence via relative humidity or vapour pressure deficit [8]. The treatment of canopy energy budgets is not considered in several models, meaning that leaf temperature is assumed to be equal to air temperature – however, this would not be expected to alter trends in WUE. Canopy phenology (the timing of leaf onset and offset), is treated explicitly by all models using the growing-degree day concept (GDD) combined with temperature and soil moisture controls. While in principle, the GDD concept is similar among models, the parameterization of such models can differ greatly and have large influences on the modeled carbon budget[49]. Vegetation distributions (at the plant functional type level for all models) are handled by either allowing for dynamic vegetation, where the PFT distributions are determined by climate and competition, or by prescribing PFT fractions based on land cover information[50].

Analysis of DGVM results. Models reported their output data at various native spatial (0.5 to 3.75 degrees) and temporal resolutions (daily, monthly, annual) from 1901-2010, and so the variables were standardized for comparison and aggregated by PFT to the European scale. When necessary (i.e., for LPJ-GUESS, which reported finer-scale categories for PFTs), the PFTs were aggregated into 6 coarser categories (broadleaf evergreen, broadleaf deciduous, needleleaf evergreen, needleleaf deciduous, C3 grass, and C4 grass), with analysis conducted for the PFTs closest matches to the empirical tree-ring datasets. In comparison to previous analysis we also place specific emphasis on the PFT-level response of the DGVMs to elucidate different processes and connections with the empirical data. In addition to the default set of model output variables requested for the TRENDY exercise, modelers were also requested to provide stomatal conductance and for internal leaf CO_2 concentrations. The model variables that were analyzed included gross primary productivity (GPP), transpiration (T), canopy stomatal conductance (Gc), leaf internal CO_2 concentration (C_i), and leaf area index (LAI). Annual GPP, T and Gc were summed for each PFT for the European continent, and mean annual C_i and LAI were averaged for each PFT. Total continental T and GPP were estimated by summing across all PFTs, whereas C_i and LAI were weighted according to their PFT fractions at the grid-cell scale. Water-use efficiency was calculated in three ways, the

first as GPP/T (WUE), the second as intrinsic water-use efficiency (GPP/Gc), and the third as inherent water-use efficiency ((GPP*VPD)/ Gc) as in ref. [51].

Supplementary Discussion on uncertainty estimation and propagation

Despite the utility of tree-ring data in investigations of the earth's coupled hydrological and carbon cycle systems[52], their use to reconstruct changes in the leaf-level processes[38,53-55] is also not without challenges. Numerous studies have shown that the isotope fractionation in leaves is closely related to the inter-cellular to atmospheric CO_2 concentration gradient[56], with carbon isotopes providing information on the balance of potential water loss and carbon assimilation (see main text). A variety of approaches have been employed in literature to reconstruct the iWUE from the annual rings of trees, including investigations considering whole wood[53], wood cellulose adjusted for a discrimination differential between bulk leaf discrimination and cellulose[38,57], and wood cellulose not considering any post photosynthetic discrimination[58]. Further differentiation of existing studies includes the use of cellulose from entire tree-rings versus latewood material[59], where signals in the latter are believed to be most free from effects related to the storage and reallocation of carbohydrates[60]. Tree-ring based reconstructions have also been performed at annual (e.g., this study), multi-year[61,62], and sub-decadal[53] resolution. Such variation in research protocols is by necessity associated with any literature review or meta-analyses[55].

In our study, we have made efforts to consider and when possible minimize uncertainties in the estimation of water use efficiency. Measurements from all sites utilize only cellulose material prepared and analyzed according to consistent laboratory standards and approaches[14]. Except for one site where narrow tree-rings did not allow this to be performed, individual tree-rings were separated at the latewood boundaries to minimize analysis of remobilized carbohydrates from photosynthesis of the previous year. Nevertheless, the exact processes and mechanisms by which leaf-level signals are transmitted and "locked" in the annual growth rings of trees is an area of active research [25,63], and contribute to the uncertainty in C_i and iWUE estimates.

The original formulation of the Farquhar isotope discrimination model[21,22] is applicable for the primary photosynthetic assimilates in the leaf and does not consider downstream post photosynthetic fractionation due to processes including synthesis of secondary sugars, respiration, compound exchange within the phloem, starch storage and subsequent remobilization and incorporation in the wood structure[23-25]. Conveniently, these post-photosynthetic processes are to some extent reflected in the compound and organ specific

fractionation, measurements of which can be used to both improve estimation of iWUE from tree ring material and quantify associated uncertainties.

We utilize a modified version of the linear Farquhar model[24,26] where the term d is employed to sum discrimination (d_1, d_2,...,d_n) beyond those associated with the direct photosynthetic production of triose phosphates and ε represents variability among trees within a site (see below). A review[23] suggests that certain stages of this post photosynthetic fractionation to be determined with relative ease, whereas other pathways remain more poorly quantified. Considering current knowledge and available data, we accordingly characterize the post-photosynthetic fractionation based upon measurements of the isotope composition available for the leaves (d_1), in the bulk wood material (d_2), and in the alpha-cellulose (d_3). Limited evidence suggests that bulk leaf/needle compositions are slightly depleted in ^{13}C relative to the primary assimilates (Figure 6 in ref. [64] and ref. [63]). We utilize a rough value of 0.5‰ with a relatively wide error range (± 1.0‰) in this study for d_1. The ^{13}C enrichment of the whole wood and other plant organs in comparison to the leaves is more readily established[65] with average depletion by 1.26‰ (and an approximate 95% confidence limit of ± 0.14‰) from a compilation of 410 reported results[66]. In our study we utilize a value of 1.3 ± 0.5‰ for this discrimination (d_2) rounding up the mean discrimination value and widening the confidence limits. Also widely reported are the differences in isotope fractionation between tree-ring cellulose and whole wood with for example enrichment in the alpha-cellulose between 0.89 – 1.68‰ for naturally grown beech, oak and spruce trees[67]. The isotope ratios of cellulose and whole wood material have been found to be consistently offset at both the intra-seasonal and inter-annual time scales[60,65] and again permit some correction for these differences when deriving C_i and iWUE estimates from tree-rings. A review of more than 100 measurements of cellulose versus the bulk mass determined an average cellulose enrichment of 1.29 ± 0.16‰ (ref. [66]). We similarly utilize a value of 1.3 ± 0.5‰ for this discrimination. To first order, the total enrichment, d, from the primary photosynthates in the leaves to the wood cellulose can be expressed as the sum of these sub component discriminations (here: d_1 = -0.5± 1.0‰; d_2 =1.3 ± 0.5‰; d_3 =1.3 ± 0.5‰) with the errors assumed to be independent and appropriately propagated in quadrature. Herein we employ an enrichment of 2.1 ± 1.2‰ from the primary photoassimilates to the wood alpha-cellulose and add this value (and uncertainty range) to the alpha-cellulose measurements to better estimate the magnitude of leaf-level processes. As the mechanistic understanding improves and more measurements become available the individual d terms can be refined, expanded upon, and uncertainties reduced. More recent estimates of

intermediate pathways such as characterization of phloem sugars also point to general post-photosynthetic fractionation in this range[25,63,64].

The above discussion considers the fractionation processes within an individual tree, however, the intensity at which these processes occur may vary among individuals within a forest stand. Observations supporting tree specific homeostatic regulation include systematic offsets between the coherent intra[63] and inter-annual[32] variability. For this reason, part of increasing the signal to noise ratio, we measured different individuals within each stand. Our sampling and measurement protocol followed the general guidelines based upon correlations of isotope measurements indicates that good agreement (e.g., EPS > 0.85 ; ref. [68]) with the theoretical population chronology is obtained by ~4 trees[16]. However, such correlation metrics do not account for systematic offset in isotope discrimination within[69] and among[70,71] trees, which may add further uncertainty to the absolute estimates of plant water use efficiency. A review of literature quantifying inter-tree variability in isotope discrimination comes up with a general 1-3‰ range for carbon isotopes[69], with a simple mean of the reported ranges yielding estimates for inter-tree variability approximately at 1.2 – 2.6‰. To better estimate the uncertainty resulting from tree-specific offsets we employ a recent dataset consisting of single tree measurements at decadal resolution spanning much of the past Millennium from the Spanish Pyrenees[71]. The inter-series range (maximum – minimum values) of 25 samples over 70 decadal periods ranges from 0.71- 3.1‰ corresponding well values in the literature. More useful however for estimating the biases related to sub-sampling from a population dataset is the standard deviation around mean, for which we obtain a mean value of 0.6‰ and a range among the different decadal intervals of 0.30 – 0.91‰ from these trees in the Spanish Pyrenees. Monte Carlo resampling trials using n=5 (accounting for some replicate measures within trees) with a standard deviation of 0.91‰ yields a 95% uncertainty in the mean isotope discrimination at a site of ± 0.8‰. We employ this as further uncertainty in the isotope discrimination model using the ε term. We consider this uncertainty a conservative measure as some of the variability associated with the leaf to cellulose discrimination (terms d_2 and d_3 above) also influence tree-to-tree variations.

Tree leaves and needles are the most important interface by which trees respond to and interact with variable atmospheric conditions, but it likely that post photosynthetic fractionation, allocation and partitioning of reserves within trees also depends upon climatic variation. In our approach, we have considered the influence of climate variation on isotope fractioning by comparisons and analysis with the optimal instrumental target for each site (see

below). These methods importantly eliminate falsely attributing all changes in tree-ring isotope fractionation to changes in atmospheric CO_2, but at present we cannot attribute these climatic signals prominently preserved in the tree-ring archive to the leaf, stem, and storage and transport processes.

Accordingly measured carbon isotope values in the alpha-cellulose were corrected for post photosynthetic discrimination of $2.1 \pm 1.5‰$ to reflect leaf level changes. The post-photosynthetic values for the alpha-cellulose and their uncertainty ranges (assumed to be normally distributed) were propagated throughout the analysis to the derived the C_i and τ. The final ^{cc}iWUE values and the associated uncertainty intervals were obtained by bootstrap sampling from the distributions of site level C_i measurements and τ estimates.

While we attempt to provide the most accurate estimates (including quantified uncertainties) of inter-cellular CO_2 concentration and water use efficiency and their changes over time, we note in conclusion that not all estimates are equally reliable. For example, the absolute changes in inter-cellular CO_2 concentration (e.g. as shown in **Figure 2a**) are more sensitive to uncertainties in both pre and post photosynthetic fractionation then the percent changes in intrinsic water use efficiency (e.g., **Figure S4**) throughout the 20th century. Estimating/removing the climatic contributions to iWUE trends and the differences in site responses contributes to the total uncertainty range in of the ^{cc}iWUE (**Figure 3a**).

Supplementary References

1   Collatz, G. J., Ball, J. T., Grivet, C. & Berry, J. A. Physiological and environmental regulation of stomatal conductance, photosynthesis and transpiration: A model that includes a laminar boundary layer. *Agricultural and Forest Meteorology* **54**, 107-136 (1991).

2   Cox, P. M., Huntingford, C. & Harding, R. A canopy conductance and photosynthesis model for use in a GCM land surface scheme. *Journal of Hydrology* **212-213**, 79-94 (1998).

3   Monteith, J. L. & Unsworth, M. H. *Principles of Environmental Physics*. (1990).

4   Cox, P. M., Huntingford, C. & Harding, R. J. A canopy conductance and photosynthesis model for use in a GCM land surface scheme. *Journal of Hydrology* **212**, 79-94, doi:10.1016/s0022-1694(98)00203-0 (1998).

5   Farquhar, G. D., von Caemmerer, S. & Berry, J. A. A biochemical model of photosynthetic CO_2 assimilation in leaves of C3 species. *Planta* **149**, 78-90 (1980).

6   Haxeltine, A. & Prentice, I. C. BIOME3: An equilibrium terrestrial biosphere model based on ecophysiological constraints, resource availability, and competition among plant functional types. *Global Biogeochemical Cycles* **10**, 693-709 (1996).

7   Monteith, J. L. Accommodation between transpiring vegetation and the convective boundary layer. *Journal of Hydrology* **166**, 251-263 (1995).

8   Ball, J. T., Woodrow, I. E. & Berry, J. A. A model predicting stomatal conductance and its contribution to the control of photosynthesis under different environmental conditions. (1987).

9   Oleson, K. W. *et al.* Technical description of version 4.0 of the Community Land Model (CLM). (2010).

10   Ducoudre, N. I., Laval, K. & Perrier, A. SECHIBA, a new set of parameterizations of the ydrlogic exchanges at the land-atmosphere interface within the LMD atmospheric general circulation model. *Journal of Climate* **6**, 248-273 (1993).

11   Leuning, R. A critical appraisal of a combined stomatal-photosynthesis model for C3 plants. *Plant, Cell and Environment* **18**, 339-355 (1995).

12   Sitch, S. *et al.* Trends and drivers of regional sources and sinks of carbon dioxide over the past two decades. *Biogeosciences Discuss.* **10**, 20113-20177, doi:10.5194/bgd-10-20113-2013 (2013).

13   Willett, K. M., Jones, P. D., Gillett, N. P. & Thorne, P. W. Recent Changes in Surface Humidity: Development of the HadCRUH Dataset. *Journal of Climate* **21**, 5364-5383, doi:10.1175/2008jcli2274.1 (2008).

14   Boettger, T. *et al.* Wood cellulose preparation methods and mass spectrometric analyses of $\delta^{13}C$, $\delta^{18}O$, and nonexchangeable δ^2H values in cellulose, sugar, and starch: An interlaboratory comparison. *Anal. Chem.* **79**, 4603-4612, doi:10.1021/ac0700023 (2007).

15   Tans, P. P., Dejong, A. F. M. & Mook, W. G. Natural atmospheric ^{14}C variation and the Suess Effect. *Nature* **280**, 826-827 (1979).

16   McCarroll, D. & Loader, N. J. Stable isotopes in tree rings. *Quaternary Science Reviews* **23**, 771-801, doi:10.1016/j.quascirev.2003.06.017 (2004).

17   Mitchell, T. D. & Jones, P. D. An improved method of constructing a database of monthly climate observations and associated high-resolution grids. *International Journal of Climatology* **25**, 693-712, doi:10.1002/joc.1181 (2005).

18   Lowe, P. & Ficke, J. Technical Paper No. 4-74. *Environmental Prediction Research Facility, Naval post-graduate school, Monterey* (1974).

19   Bonan, G. B. *Ecological climatology: concepts and applications*. (Cambridge University Press, 2002).

20   van der Schrier, G., Briffa, K. R., Jones, P. D. & Osborn, T. J. Summer moisture variability across Europe. *Journal of Climate* **19**, 2818-2834 (2006).

21   Farquhar, G. D., Oleary, M. H. & Berry, J. A. On the relationship between carbon isotope discrimination and the inter-cellular carbon-dioxide concentration in leaves. *Aust. J. Plant Physiol.* **9**, 121-137 (1982).

22   Farquhar, G. D., Ehleringer, J. R. & Hubick, K. T. Carbon isotope discrimination and photosynthesis. *Annu. Rev. Plant Physiol. Plant Molec. Biol.* **40**, 503-537 (1989).

23   Brüggemann, N. *et al.* Carbon allocation and carbon isotope fluxes in the plant-soil-atmosphere continuum: a review. *Biogeosciences* **8**, 3457-3489, doi:10.5194/bg-8-3457-2011 (2011).

24   Cernusak, L. A. *et al.* Viewpoint: Why are non-photosynthetic tissues generally ^{13}C enriched compared with leaves in C-3 plants? Review and synthesis of current hypotheses. *Functional Plant Biology* **36**, 199-213, doi:10.1071/fp08216 (2009).

25   Gessler, A. *et al.* Tracing carbon and oxygen isotope signals from newly assimilated sugars in the leaves to the tree-ring archive. *Plant Cell Environ.* **32**, 780-795, doi:10.1111/j.1365-3040.2009.01957.x (2009).

26   Hubick, K. T., Farquhar, G. D. & Shorter, R. Correlation between water-use efficiency and carbon isotope discrimination in diverse peanut (Arachis) germplasm. *Aust. J. Plant Physiol.* **13**, 803-816 (1986).

27   Schubert, B. A. & Jahren, A. H. The effect of atmospheric CO_2 concentration on carbon isotope fractionation in C-3 land plants. *Geochim. Cosmochim. Acta* **96**, 29-43, doi:10.1016/j.gca.2012.08.003 (2012).

28   Flexas, J., Ribas-Carbo, M., Diaz-Espejo, A., Galmes, J. & Medrano, H. Mesophyll conductance to CO_2: current knowledge and future prospects. *Plant Cell Environ.* **31**, 602-621, doi:10.1111/j.1365-3040.2007.01757.x (2008).

29   Beer, C. *et al.* Temporal and among-site variability of inherent water use efficiency at the ecosystem level. *Glob. Biogeochem. Cycle* **23**, doi:10.1029/2008gb003233 (2009).

30   Treydte, K. S. *et al.* Impact of climate and CO_2 on a millennium-long tree-ring carbon isotope record. *Geochim. Cosmochim. Acta* **73**, 4635-4647, doi:10.1016/j.gca.2009.05.057 (2009).

31   Treydte, K. S. *et al.* The twentieth century was the wettest period in northern Pakistan over the past millennium. *Nature* **440**, 1179-1182, doi:10.1038/nature04743 (2006).

32   Kress, A. *et al.* A 350 year drought reconstruction from Alpine tree ring stable isotopes. *Glob. Biogeochem. Cycle* **24**, 1-16, doi:Gb2011 10.1029/2009gb003613 (2010).

33   Rinne, K. T., Loader, N. J., Switsur, V. R., Treydte, K. S. & Waterhouse, J. S. Investigating the influence of sulphur dioxide (SO_2) on the stable isotope ratios ($\delta^{13}C$ and $\delta^{18}O$) of tree rings. *Geochim. Cosmochim. Acta* **74**, 2327-2339, doi:10.1016/j.gca.2010.01.021 (2010).

34   Böhm, R. *et al.* The early instrumental warm-bias: a solution for long central European temperature series 1760-2007. *Climatic Change* **101**, 41-67, doi:10.1007/s10584-009-9649-4 (2010).

35   Ainsworth, E. A. & Rogers, A. The response of photosynthesis and stomatal conductance to rising [CO_2]: mechanisms and environmental interactions. *Plant Cell Environ.* **30**, 258-270, doi:10.1111/j.1365-3040.2007.01641.x (2007).

36   Boettger, T., Haupt, M., Friedrich, M. & Waterhouse, J. S. Reduced climate sensitivity of carbon, oxygen and hydrogen stable isotope ratios in tree-ring cellulose of silver fir (Abies alba Mill.) influenced by background SO2 in Franconia (Germany, Central Europe). *Environmental Pollution* **185**, 281–294 (2014).

37   Frank, D., Büntgen, U., Bohm, R., Maugeri, M. & Esper, J. Warmer early instrumental measurements versus colder reconstructed temperatures: shooting at a moving target. *Quat. Sci. Rev.* **26**, 3298-3310 (2007).

38   Saurer, M. *et al.* Spatial variability and temporal trends in water-use efficiency of European forests. *Global Change Biology* (in revision).

39   Sitch, S. *et al.* Evaluation of ecosystem dynamics, plant geography and terrestrial carbon cycling in the LPJ dynamic global vegetation model. *Global Change Biology* **9**, 161-185 (2003).

40   Smith, B., Prentice, I. C. & Sykes, M. T. Representation of vegetation dynamics in the modelling of terrestrial ecosystems: comparing two contrasting approaches within European climate space. *Global Ecology and Biogeography* **10**, 621-637, doi:10.1046/j.1466-822X.2001.t01-1-00256.x (2001).

41   Woodward, F. I. & Lomas, M. R. Vegetation dynamics – simulating responses to climatic change. *Biological Reviews* **79**, 643-670, doi:doi:10.1017/S1464793103006419 (2004).

42   Krinner, G. *et al.* A dynamic global vegetation model for studies of the coupled atmosphere-biosphere system. *Glob. Biogeochem. Cycle* **19**, doi:10.1029/2003gb002199 (2005).

43   Oleson, K. *et al.* Improvements to the Community Land Model and their impact on the hydrological cycle. *J. Geophys. Res* **113**, G01021 (2008).

44   Piao, S. *et al.* Evaluation of terrestrial carbon cycle models for their response to climate variability and to CO_2 trends. *Global Change Biology* **19**, 2117-2132, doi:10.1111/gcb.12187 (2013).

45   Hurtt, G. C. *et al.* Harmonization of land-use scenarios for the period 1500–2100: 600 years of global gridded annual land-use transitions, wood harvest, and resulting secondary lands. *Climatic Change* (2011).

46   Zobler, L. A world soil file for global climate modeling. *NASA Technical Memorandum*, 32 pp (1986).

47   Bernacchi, C. J., Kimball, B. A., Quarles, D. R., Long, S. P. & Ort, D. R. Decreases in stomatal conductance of soybean under open-air elevation of $[CO_2]$ are closely coupled with decreases in ecosystem evapotranspiration. *Plant Physiol.* **143**, 134-144, doi:10.1104/pp.106.089557 (2007).

48   Farquhar, G. D., Caemmerer, S. & Berry, J. A biochemical model of photosynthetic CO_2 assimilation in leaves of C3 species. *Planta* **149**, 78-90 (1980).

49   Richardson, A. D. *et al.* Terrestrial biosphere models need better representation of vegetation phenology: results from the North American Carbon Program Site Synthesis. *Global Change Biology* **18**, 566-584 (2012).

50   Poulter, B. *et al.* Plant functional type mapping for earth system models. *Geoscientific Model Development Discussions* **4**, 1-41 (2011).

51   Beer, C. *et al.* Temporal and among-site variability of inherent water use efficiency at the ecosystem level. *Global Biogeochemical Cycles* **23**, DOI:10.1029/2008GB003233 (2009).

52   Frank, D. C. *et al.* Ensemble reconstruction constraints on the global carbon cycle sensitivity to climate. *Nature* **463**, 527-530, doi:10.1038/nature08769 (2010).

53   Saurer, M., Siegwolf, R. T. W. & Schweingruber, F. H. Carbon isotope discrimination indicates improving water-use efficiency of trees in northern Eurasia over the last 100 years. *Global Change Biology* **10**, 2109-2120, doi:10.1111/j.1365-2486.2004.00869.x (2004).

54   Feng, X. H. Trends in intrinsic water-use efficiency of natural trees for the past 100-200 years: A response to atmospheric CO_2 concentration. *Geochim. Cosmochim. Acta* **63**, 1891-1903 (1999).

55   Peñuelas, J., Canadell, J. G. & Ogaya, R. Increased water-use efficiency during the 20th century did not translate into enhanced tree growth. *Global Ecology and Biogeography* **20**, 597-608, doi:10.1111/j.1466-8238.2010.00608.x (2011).

56   Brugnoli, E., Hubick, K. T., von Caemmerer, S., Wong, S. C. & Farquhar, G. D. Correlation between the Carbon Isotope Discrimination in Leaf Starch and Sugars of C3 Plants and the Ratio of Intercellular and Atmospheric Partial Pressures of Carbon Dioxide. *Plant Physiol.* **88**, 1418-1424, doi:10.1104/pp.88.4.1418 (1988).

57   Nock, C. A. *et al.* Long-term increases in intrinsic water-use efficiency do not lead to increased stem growth in a tropical monsoon forest in western Thailand. *Global Change Biology* **17**, 1049-1063, doi:10.1111/j.1365-2486.2010.02222.x (2011).

58   Andreu-Hayles, L. *et al.* Long tree-ring chronologies reveal 20th century increases in water-use efficiency but no enhancement of tree growth at five Iberian pine forests. *Global Change Biology* **17**, 2095-2112, doi:10.1111/j.1365-2486.2010.02373.x (2011).

59   Waterhouse, J. S. *et al.* Northern European trees show a progressively diminishing response to increasing atmospheric carbon dioxide concentrations. *Quaternary Science Reviews*, 803-810, doi:10.1016/j.quascirev.2003.06.011 (2004).

60   Helle, G. & Schleser, G. H. Beyond CO2-fixation by Rubisco - an interpretation of C-13/C-12 variations in tree rings from novel intra-seasonal studies on broad-leaf trees. *Plant Cell Environ.* **27**, 367-380, doi:10.1111/j.0016-8025.2003.01159.x (2004).

61   Penuelas, J., Hunt, J. M., Ogaya, R. & Jump, A. S. Twentieth century changes of tree-ring delta C13 at the southern range-edge of Fagus sylvatica: increasing water-use efficiency does not avoid the growth decline induced by warming at low altitudes. *Global Change Biology* **14**, 1076-1088, doi:10.1111/j.1365-2486.2008.01563.x (2008).

62   Knapp, P. A. & SoulÉ, P. T. Increasing water-use efficiency and age-specific growth responses of old-growth ponderosa pine trees in the Northern Rockies. *Global Change Biology* **17**, 631-641, doi:10.1111/j.1365-2486.2010.02209.x (2011).

63   Offermann, C. *et al.* The long way down—are carbon and oxygen isotope signals in the tree ring uncoupled from canopy physiological processes? *Tree Physiology* **31**, 1088-1102, doi:10.1093/treephys/tpr093 (2011).

64   Gessler, A., Tcherkez, G., Peuke, A. D., Ghashghaie, J. & Farquhar, G. D. Experimental evidence for diel variations of the carbon isotope composition in leaf, stem and phloem sap organic matter in Ricinus communis. *Plant, Cell & Environment* **31**, 941-953, doi:10.1111/j.1365-3040.2008.01806.x (2008).

65   Leavitt, S. W. & Long, A. Evidence for 13C/12C fractionation between tree leaves and wood. *Nature* **298**, 742-744 (1982).

66   Badeck, F.-W., Tcherkez, G., Nogués, S., Piel, C. & Ghashghaie, J. Post-photosynthetic fractionation of stable carbon isotopes between plant organs—a widespread phenomenon. *Rapid Communications in Mass Spectrometry* **19**, 1381-1391, doi:10.1002/rcm.1912 (2005).

67   Borella, S., Leuenberger, M., Saurer, M. & Siegwolf, R. Reducing uncertainties in $\delta^{13}C$ analysis of tree rings: Pooling, milling, and cellulose extraction. *Journal of Geophysical Research-Atmospheres* **103**, 19519-19526 (1998).

68   Wigley, T. M. L., Briffa, K. R. & Jones, P. D. On the average value of correlated time-series, with applications in dendroclimatology and hydrometeorology. *Journal of Climate and Applied Meteorology* **23**, 201-213, doi:10.1175/1520-0450(1984)023<0201:otavoc>2.0.co;2 (1984).

69   Leavitt, S. W. Tree-ring C–H–O isotope variability and sampling. *Science of The Total Environment* **408**, 5244-5253, doi:http://dx.doi.org/10.1016/j.scitotenv.2010.07.057 (2010).

70   Hangartner, S., Kress, A., Saurer, M., Frank, D. & Leuenberger, M. Methods to merge overlapping tree-ring isotope series to generate multi-centennial chronologies. *Chemical Geology* **294–295**, 127-134, doi:http://dx.doi.org/10.1016/j.chemgeo.2011.11.032 (2012).

71   Esper, J. *et al.* Low-frequency noise in delta C-13 and delta O-18 tree ring data: A case study of Pinus uncinata in the Spanish Pyrenees. *Glob. Biogeochem. Cycle* **24**, doi:10.1029/2010gb003772 (2010).